Electronic Supplementary Material (ESI) for Journal of Materials Chemistry C.

Supporting Information

Potential Molecular Qubits of Long Coherence Time Constructed by Bromo-substituted Trityl Radicals

Yu-Shuang Zhang[#], Yi-Fei Fan[#], Xing-Quan Tao, Geng-Yuan Li, Qing-Song Deng, Zheng Liu, Ye-Xin Wang*, Song Gao and Shang-Da Jiang*

Supporting Information

Contents

SI 1: General methods of synthesis, characterization and sample preparation

In this work, we reported a new bromo-substitute trityl radical 6,6'-((2,4,6-tribromophenyl) methylene) bis (1,2,3,4,5-pentachlorobenzene) (**$TBr_3Cl_{10}M$**). This radical presents three bromine atoms in o*tho*- and *para*-positions of one phenyl ring while chlorine atoms replace all of hydrogen atoms in the remaining two phenyl rings. Thus, a mixed halogen substituted trityl radical was prepared and the relevant characterizations are as follows.

Synthetic Procedure

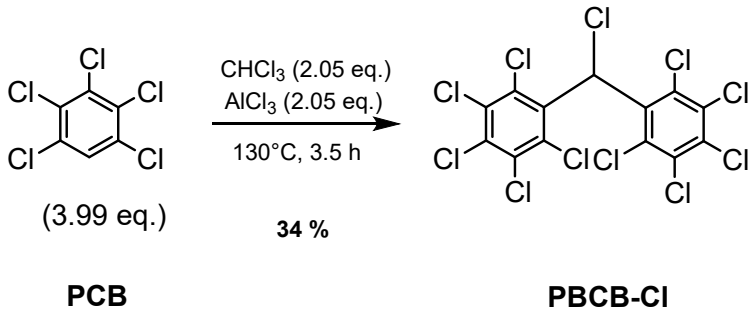

Scheme S1. Synthesis of **PBCB-Cl**[1].

Procedure: In a 25 mL high-pressure reactor equipped with a magnetic stirrer, under nitrogen flux, were added 1.0 g of 1,2,3,4,5-pentachlorobenzene (3.99 mmol), 310 mg anhydrous aluminum bromide (2.05 mmol), and 165 μL of chloroform (2.05 mmol). The mixture was heated at 130 °C for 3.5 h. The mixture was then poured on 50 mL of water and extracted with dichloromethane. The organic phase was washed with 1M hydrochloric acid (50 mL) and aqueous solution of $NaHCO_3$ (10% w/w) (50 mL) in portions, dried over Na_2SO_4 and concentrated under vacuum. The crude product was purified by column flash-chromatography on silica gel using hexane as eluent. The crude product of 6,6'-(chloromethylene) bis (1,2,3,4,5-pentachlorobenzene) (**PBCB-Cl**) was obtained as a white compound (yield = 45%).

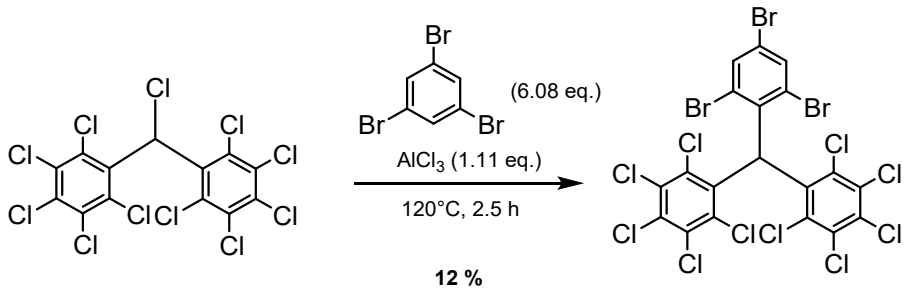

PBCB-Cl **$TBr_3Cl_{10}M$-αH**

Scheme S2. Synthesis of 6,6'-((2,4,6-tribromophenyl) methylene) bis(1,2,3,4,5-pentachlorobenzene) (**$TBr_3Cl_{10}M$-αH**).

Procedure: In a 100 mL high-pressure reactor 200 mg **PBCB-Cl** (0.36 mmol), 700 mg 1,3,5-tribromobenzene (2.19 mmol) and 60 mg anhydrous aluminum chloride (0.4 mmol) were added. The mixture was heated to 120 °C for 2.5 h. After cooling to room temperature, the mixture was poured on 50 mL of water and extracted with dichloromethane. The organic phase was washed with 1M hydrochloric acid (50 mL) and aqueous solution of $NaHCO_3$ (10% w/w) (50 mL) in portions, dried over Na_2SO_4 and concentrated under vacuum. The crude product was purified by silica gel column chromatography using cold dichloromethane as eluent. The crude product was then triturated with cold chloroform (3 x 3 mL) and centrifugated to obtain the pure white product of **$TBr_3Cl_{10}M$-αH** (yield = 12%). ^{1}H-NMR (400 MHz, $CDCl_3$), reported in Figure S1, presents the following signals: δ = 6.80 (s, 1H), δ = 7.68 (d, J = 1.8 Hz, 1H) and δ = 7.76 (d, J = 1.5 Hz, 1H). ^{13}C NMR (100 MHz, $CDCl_3$), reported in Figure S2, presents the following peaks: δ = 63.71, 122.14, 128.16, 129.25, 135.76, 137.13, 137.47 ppm. MALDI-TOF (m/z) for [TBr_3Cl_{10}M-αH]: 824.46 $[M]^+$. IR-ATR (Fig. S5): ν_{MAX} 678, 718, 756, 799, 808, 861, 1243, 1299, 1324, 1347, 1372, 1531, 1559, 1525 cm^{-1}.

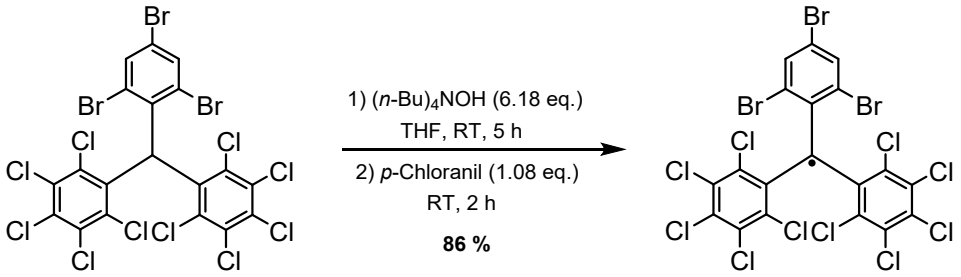

$TBr_3Cl_{10}M$-αH **$TBr_3Cl_{10}M$**

Scheme S3. Synthesis of 6,6'-((2,4,6-tribromophenyl) methylene) bis(1,2,3,4,5-pentachlorobenzene) radical (**$TBr_3Cl_{10}M$**).

Procedure: In a 25 mL high-pressure reactor equipped with a magnetic stirrer, under nitrogen flux, operating in the dark, were added 50 mg 6,6'-((2,4,6-tribromophenyl) methylene)bis(1,2,3,4,5-pentachlorobenzene) (**$TBr_3Cl_{10}M$-αH**) (0.061 mmol), 10 mL freshly distilled THF and 200 mL methanol solution of N(*n*-Bu)$_4$OH (40% w/w) (0.377 mol). After 5 h, 20 mg tetrachloro-1,4-benzoquinone (0.08 mmol) were added. After 2 h the mixture was concentrated under vacuum. The crude product was purified by column flash chromatography on silica gel using hexane: dichloromethane (3:1) as eluent, obtaining a dark-red powder product of **$TBr_3Cl_{10}M$** (R = 86%). MALDI-TOF (m/z) for [$TBr_3Cl_{10}M$]: 823.47 $[M]^+$. IR-ATR (Fig. S8): ν_{MAX} 717, 729, 861, 1260, 1304, 1333, 1548 cm^{-1}.

Structural Characterization

NMR Spectrum

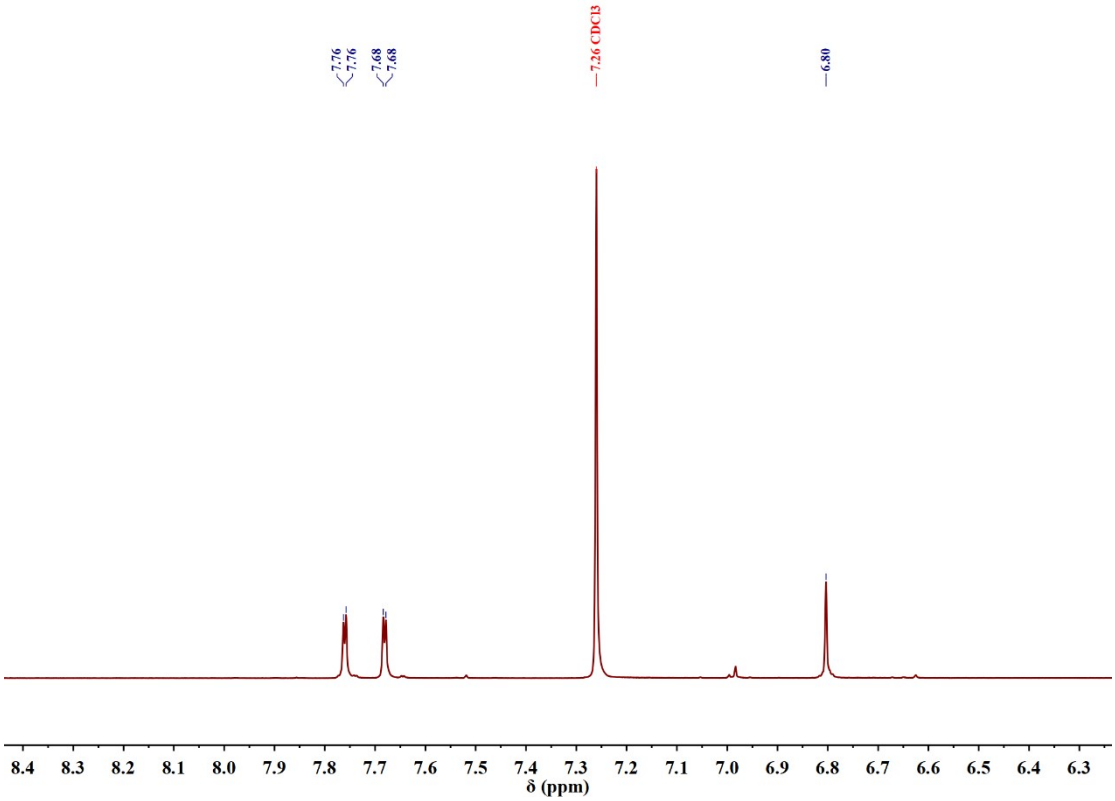

Figure S1. ^{1}H-NMR ($CDCl_3$, 400 MHz) spectrum of **TBr_3Cl_{10}M-αH**.

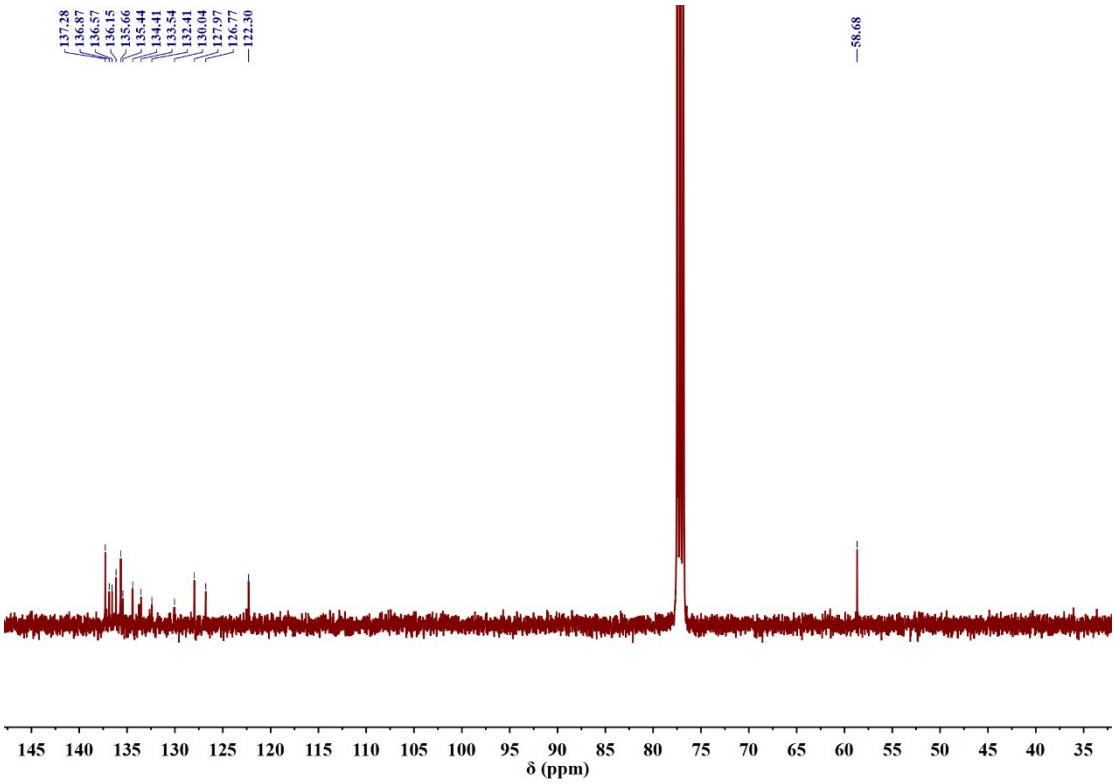

Figure S2. ^{13}C-NMR ($CDCl_3$, 100 MHz) spectrum of **TBr_3Cl_{10}M-αH**.

Mass Spectrum

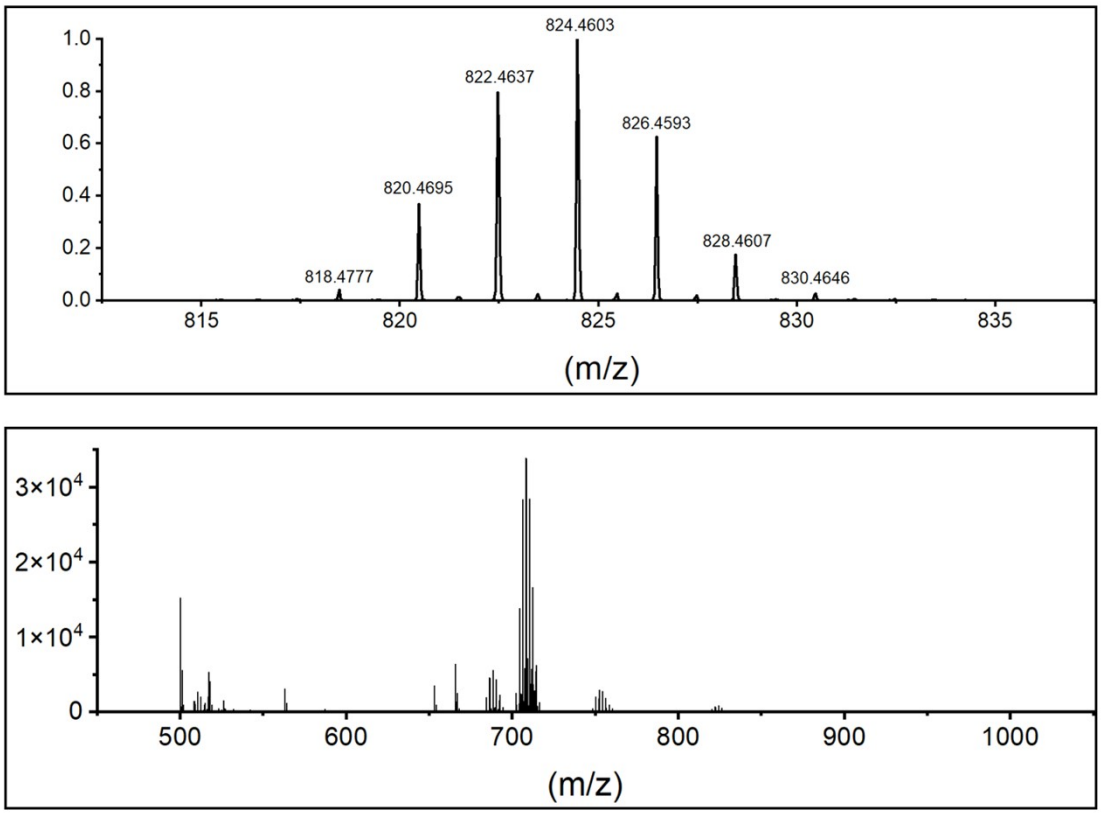

Figure S3. MALDI-TOF spectrum of **$TBr_3Cl_{10}M$-αH**.

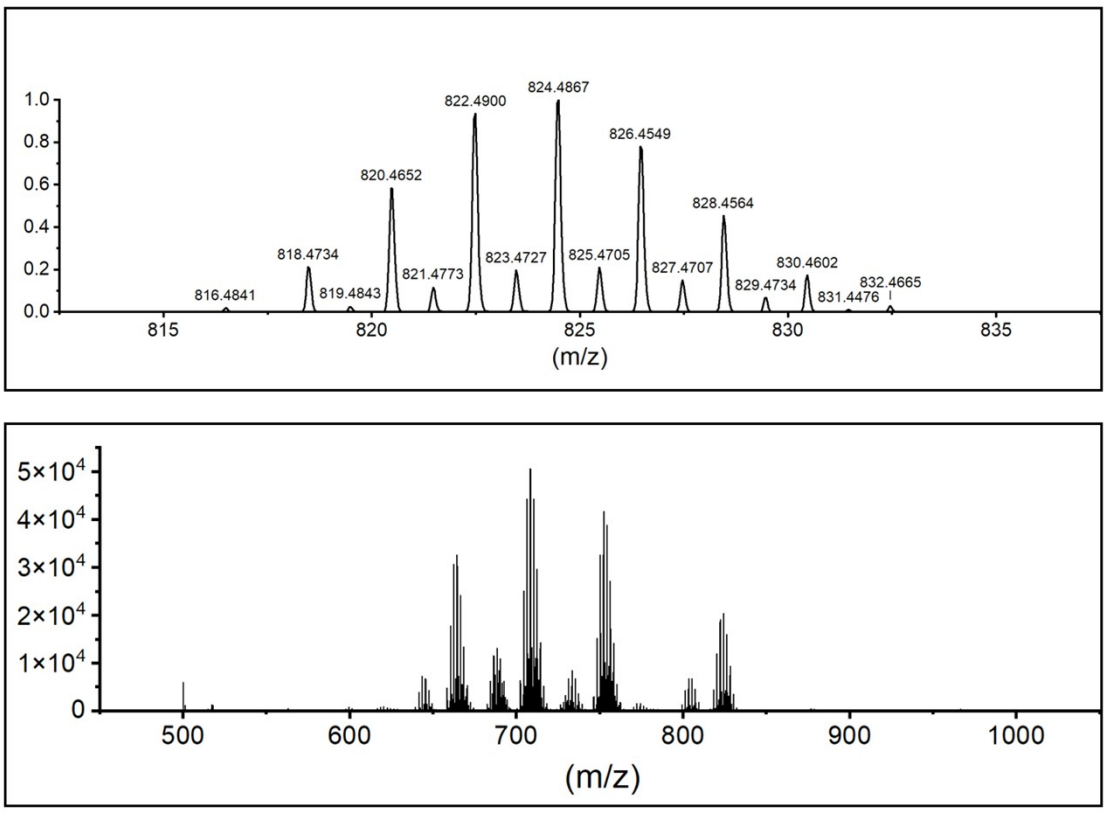

Figure S4. MALDI-TOF spectrum of **$TBr_3Cl_{10}M$**.

IR-ATR Spectrum

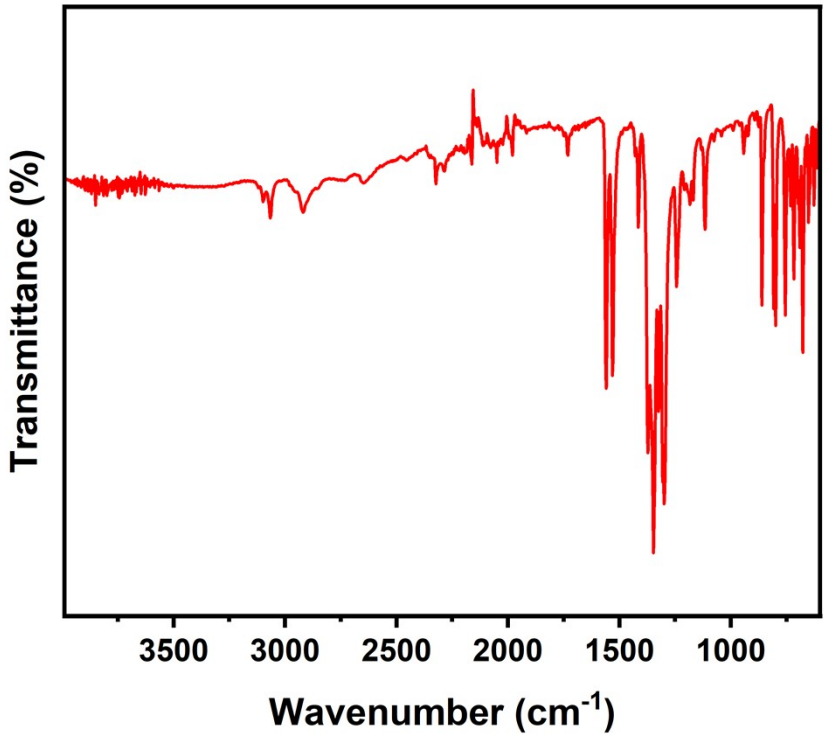

Figure S5. IR-ATR spectrum of **$TBr_3Cl_{10}M$-αH** powder.

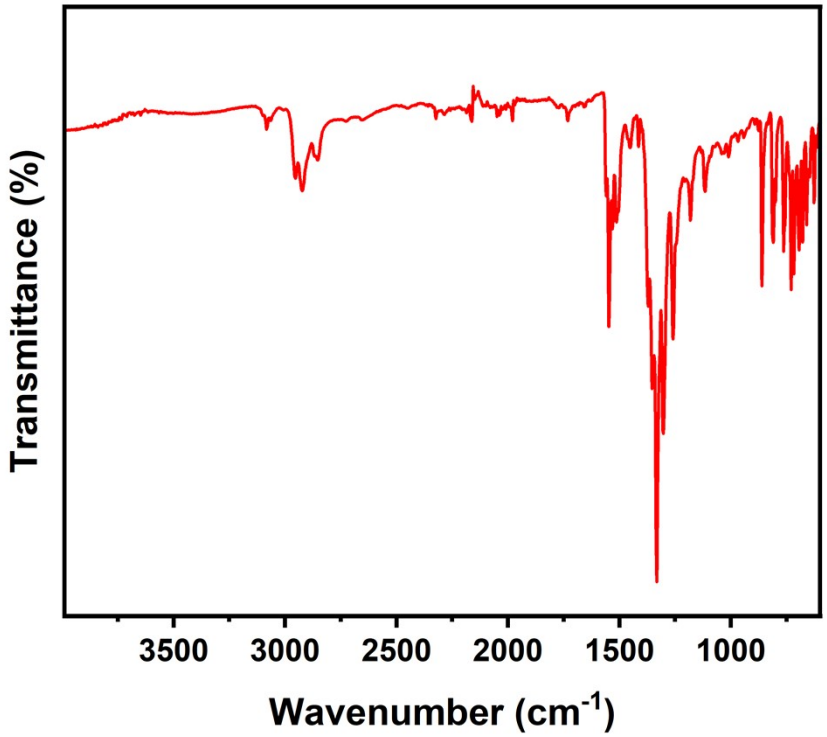

Figure S6. IR-ATR spectrum of **$TBr_3Cl_{10}M$** powder.

X-ray single crystal diffraction spectrum

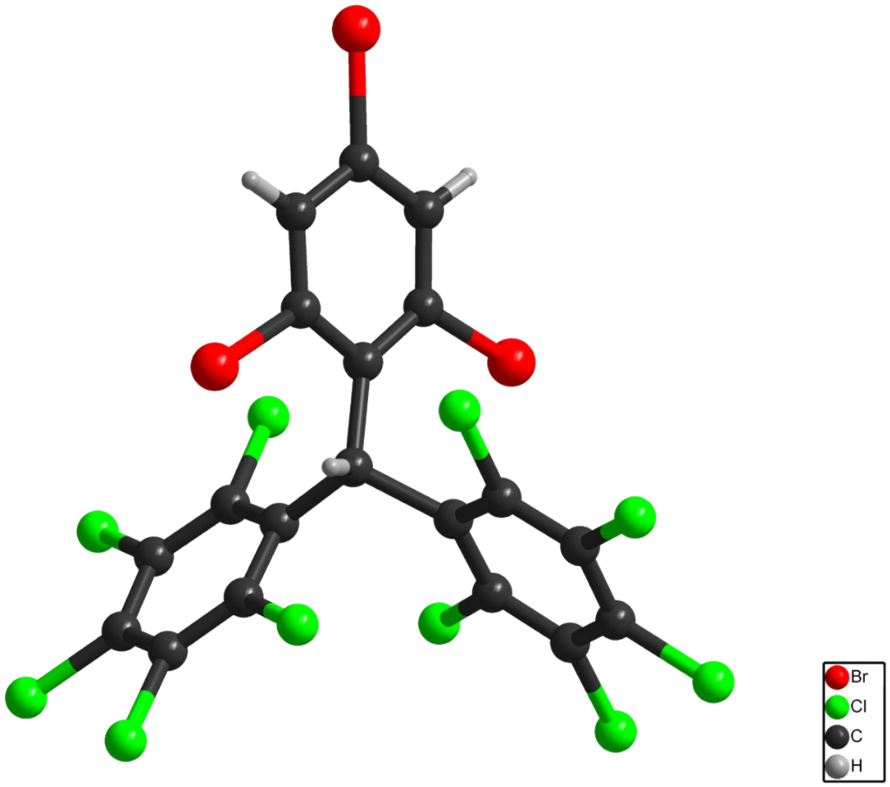

Figure S7. Molecular structures of **$TBr_3Cl_{10}M$-αH** obtained by single crystal X-Ray Diffraction.

Table S1. Crystallographic data of **$TBr_3Cl_{10}M$-αH**.

$TBr_3Cl_{10}M$-αH	
Formula	$C_{19}H_{13}Br_3Cl_{10}$
*M*r	807.39
T/*K*	150
Crystal system	Monoclinic
Space group	*C 1 2 / c 1* (No.15)
a / Å	12.8567 (3)
b / Å	11.4178 (2)
c / Å	17.8798 (4)
V / Å^3	2464.56 (10)
α / °	90
β / °	110.116 (2)
γ / °	90
Z	4
ρ_{calc} / g·cm^{-3}	2.176
μ / mm^{-1}	15.96
F_{000}	1543
Crystal size / mm^3	0.13 × 0.12 × 0.1
Radiation	Cu *K*α (λ = 1.54184 Å)
2θ range / °	2.6-76.5
R_{int}	0.0094
S (on F^2)	1.083
R_1, wR_2 ($I \geq 2\sigma(I)$)	0.0998 (2127), 0.2550 (2179)
$\Delta\rho_{max}/\Delta\rho_{min}$ / e·Å^{-3}	1.10 / -1.57

Sample Preparation

The solution samples were prepared by dissolving the radicals in degassed d_8-toluene with a concentration of 0.1 mmol/L. The film samples were prepared by mixing the radicals and PMMA in DCM with a concentration of 0.01 (w/w) and evaporating the solvent in a vacuum oven at 40 ℃ for 12 h in the dark. The film samples of TRs were scratched from substrates by knife and put into EPR tubes.

Based on the concentration of samples in PMMA film and d_8-toluene frozen solution, the average intermolecular distances and the dipole interactions are estimated by Eq. S1. The values of dipolar coupling are shown in Table S2.

$$\hat{H} = -\frac{\mu_0 \gamma_1 \gamma_2 \hbar^2}{4\pi |\vec{r}|^3}\left[3(\hat{S}_1 \cdot \vec{r})(\hat{S}_2 \cdot \vec{r}) - \hat{S}_1 \cdot \hat{S}_2\right] \#(Eq.S1)\#$$

where

H is potential energy of the interaction;

μ_0 is vacuum magnetic permeability;

$\gamma_{1,2}$ are gyromagnetic ratio of two electrons;

$S_{1,2}$ are spin quanta of two spin centers;

$|\vec{r}|$ is average distance of intermolecular;

$\hbar$ is reduced Planck constant;

$\vec{r}$ is a unit vector parallel to the line joining the centers of the two dipoles.

Table S2. Estimated dipolar interactions of samples in PMMA and d_8-toluene solutions.

PMMA Samples	Concentration (mmol/L)	Average intermolecular distance (nm)	Dipolar coupling (MHz)
PTM	15.65	4.734	0.4894
TTM	21.50	4.259	0.6721
$TBr_3Cl_{10}M$	14.42	4.865	0.4509
TBr_3Cl_6M	17.32	4.577	0.5415
TBr_6Cl_5M	13.37	4.988	0.4184
TTBrM	12.47	5.106	0.3900
Solution Samples	0.10	25.51	0.0031

Although the intermolecular dipole coupling in the PMMA samples are larger than that in d_8-toluene solutions, the interaction intensities are all less than 1 MHz. Thus, the influence of dipole interactions could be neglected.

SI 2: Simulations of CW-EPR and EDFS spectrum for TRs

Table S3. CW-EPR spectra simulation of *g*-factors and spectral linewidth of TRs in 0.1 mmol/L d_8-toluene solutions at room temperature. (*a*: $|A_{iso}|$= 3.48 MHz)

Compound	g_{iso}	Linewidth (mT)
PTM	2.0037	0.16
TTM[a]	2.0040	0.15
$TBr_3Cl_{10}M$	2.0054	0.34
TBr_3Cl_6M	2.0055	0.46
TBr_6Cl_5M	2.0065	0.43
TTBrM	2.0077	0.63

Table S4. CW-EPR spectra simulation of *g*-factors and spectral linewidth of TRs in 0.01 (w/w) PMMA films at room temperature.

Compound	$g_{eff,x}$	$g_{eff,y}$	$g_{eff,z}$	Δg (g_{max} - g_{min})	Linewidth (mT)
PTM	2.0020	2.0020	2.0057	0.0037	0.56
TTM	2.0028	2.0028	2.0058	0.0030	0.72
$TBr_3Cl_{10}M$	2.0003	2.0025	2.0107	0.0104	1.43
TBr_3Cl_6M	1.9995	2.0040	2.0111	0.0116	1.34
TBr_6Cl_5M	2.0020	2.0020	2.0134	0.0114	2.26
TTBrM	2.0024	2.0040	2.0191	0.0167	2.85

Table S5. EDFS spectra simulation of *g*-factors and spectral linewidth of TRs in 0.1 mmol/L d_8-toluene frozen solutions in glassy state at 10 K.

Compound	$g_{eff,x}$	$g_{eff,y}$	$g_{eff,z}$	Δg (g_{max} - g_{min})	Linewidth (mT)
$TBr_3Cl_{10}M$	1.9986	2.0040	2.0116	0.0130	1.51

TBr_3Cl_6M	2.0046	2.0048	2.0061	0.0015	1.99
TBr_6Cl_5M	2.0012	2.0019	2.0143	0.0131	2.35
TTBrM	2.0030	2.0033	2.0180	0.0150	3.15

Table S6. EDFS spectra simulation of *g*-factors and spectral linewidth of TRs in 0.01 (w/w) PMMA films at 10 K.

Compound	$g_{eff,x}$	$g_{eff,y}$	$g_{eff,z}$	Δg (g_{max} - g_{min})	**Linewidth (mT)**
PTM	2.0022	2.0023	2.0068	0.0047	0.64
TTM	2.0039	2.0042	2.0052	0.0012	1.02
$TBr_3Cl_{10}M$	1.9981	2.0034	2.0128	0.0147	1.66
TBr_3Cl_6M	2.0048	2.0051	2.0061	0.0013	2.39
TBr_6Cl_5M	2.0040	2.0040	2.0125	0.0085	3.37
TTBrM	1.9950	2.0156	2.0157	0.0206	3.60

Table S7. EDFS spectra simulation of g-factors and spectral linewidth of TRs in 0.01 (w/w) PMMA films at room temperature.

Compound	$g_{eff,x}$	$g_{eff,y}$	$g_{eff,z}$	Δg (g_{max} - g_{min})	**Linewidth (mT)**
PTM	2.0016	2.0016	2.0076	0.0060	0.59
TTM	2.0048	2.0051	2.0115	0.0067	0.80
$TBr_3Cl_{10}M$	2.0001	2.0004	2.0105	0.0104	1.46
TBr_3Cl_6M	2.0046	2.0047	2.0057	0.0011	2.13
TBr_6Cl_5M	2.0007	2.0009	2.0187	0.0180	2.46
TTBrM	1.9983	2.0148	2.0150	0.0167	3.60

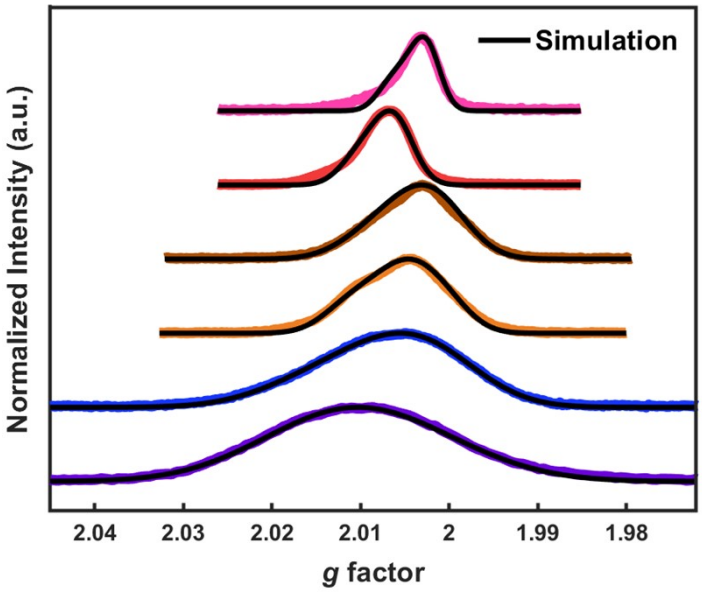

Figure S8. EDFS spectra of TRs in 0.01 (w/w) PMMA films at room temperature.

SI 3: T_1 measurement and fitting for TRs

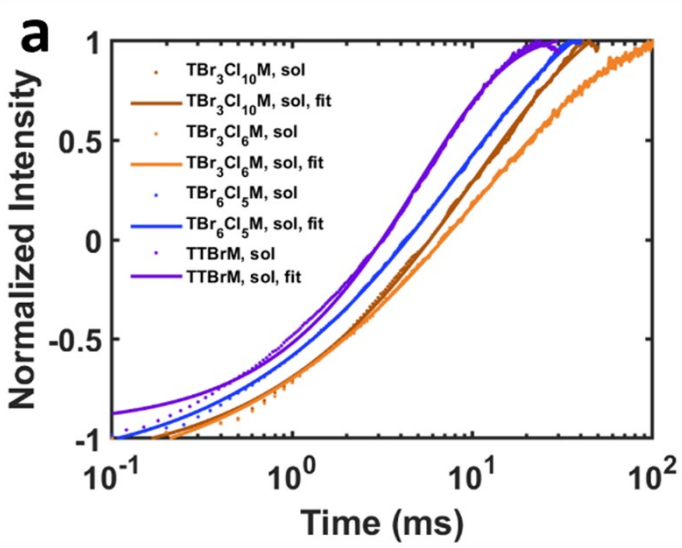

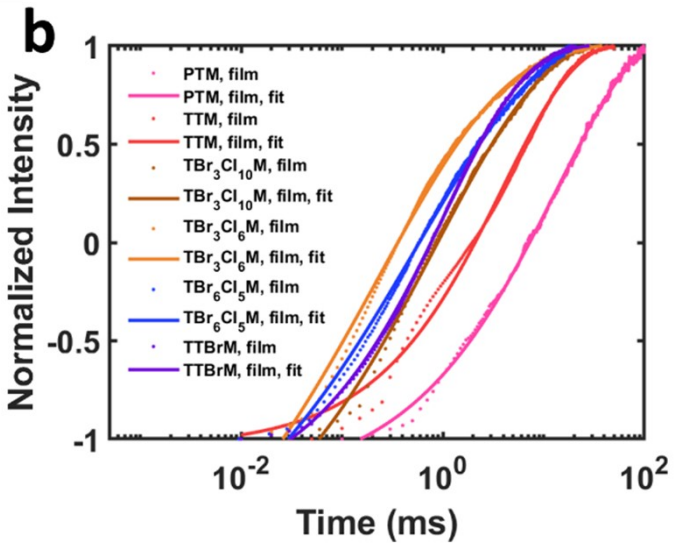

Figure S9. a) T_1 of TRs in 0.1 mmol/L d_8-toluene frozen solutions in glassy state at 10 K and b) 0.01 (w/w) PMMA films at 10 K. (The data was smoothed with a five-point moving average).

All the inversion recovery data are fitted with the stretched exponential decay function in Eq. S2,

$$I(t) = I(0)\exp\left(-\frac{t}{T}\right)^{x} \#(Eq.S2)\#$$

For the clarity of the graphs, we kept only the raw data and omitted the fitted curves in the following graphs.

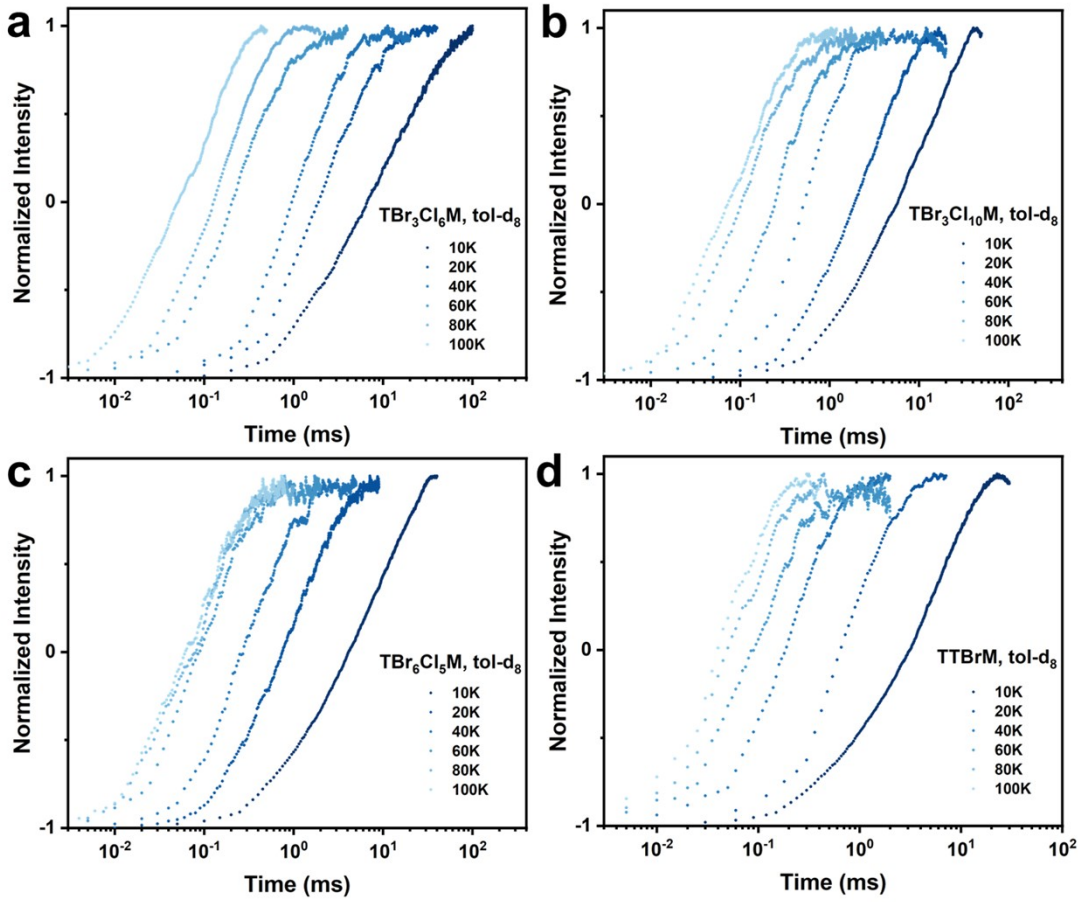

Figure S10. Variable temperature inversion recovery data of TRs a) **TBr_3Cl_6M**, b) **$TBr_3Cl_{10}M$**, c) **TBr_6Cl_5M** and d) **TTBrM** in 0.1 mmol/L d_8-toluene frozen solution in glassy state (The data was smoothed with a five-point moving average).

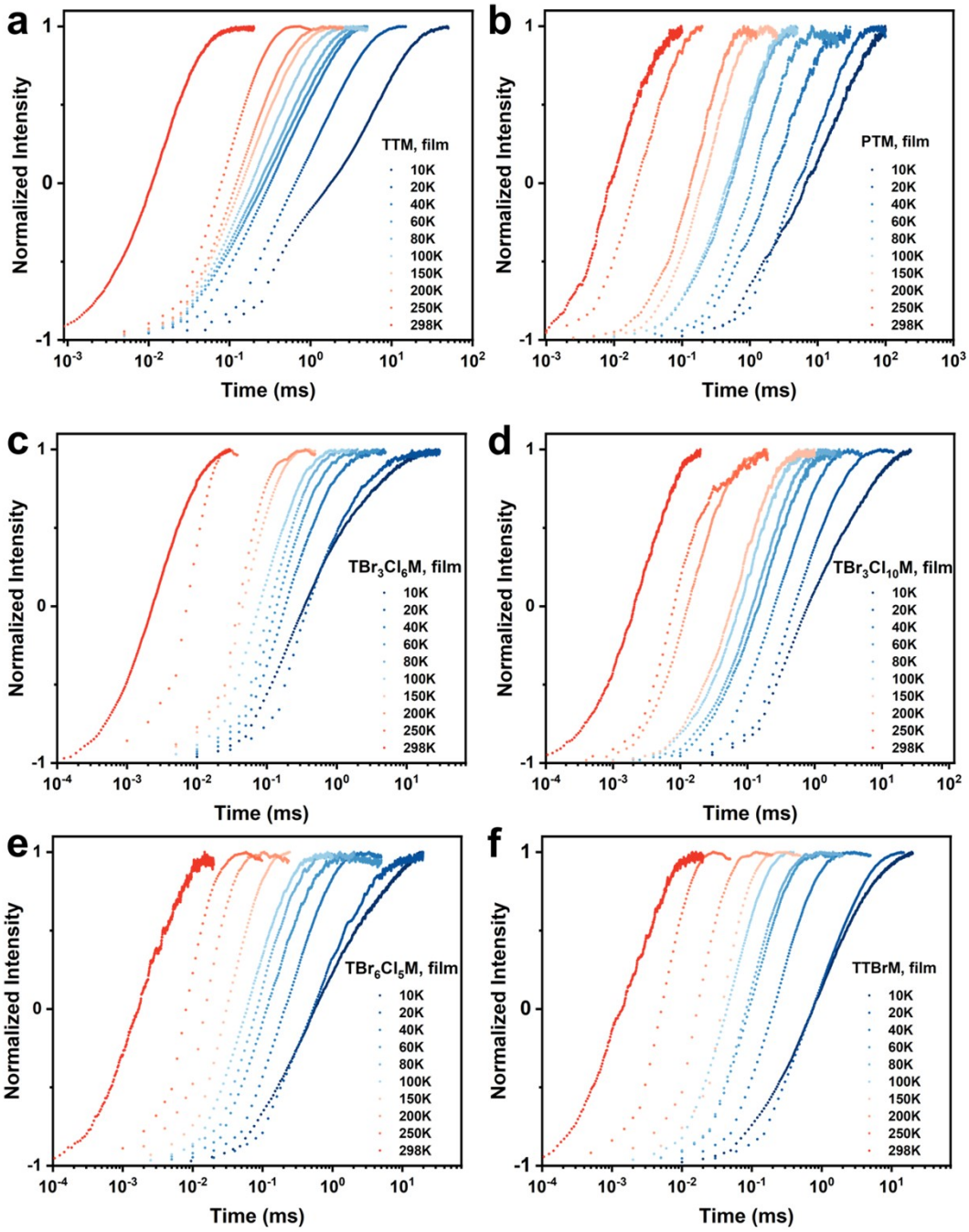

Figure S11. Variable temperature inversion recovery data of TRs a) **TTM**, b) **PTM**, c) **TBr_3Cl_6M**, d) **$TBr_3Cl_{10}M$**, e) **TBr_6Cl_5M** and f) **TTBrM** in 0.01 (w/w) PMMA films (The data was smoothed with a five-point moving average).

Table S8. Variable temperature T_1 values of TRs in 0.1 mmol/L d_8-toluene solutions.

$TBr_3Cl_{10}M$, sol.		**TBr_3Cl_6M, sol.**		**TBr_6Cl_5M, sol.**		**TTBrM, sol.**	
***T* / K**	**T_1/ ms**	***T* / K**	**T_1/ ms**	***T* / K**	**T_1/ ms**	***T* / K**	**T_1/ ms**
10	10.6(2)	10	10.9(1)	10	8.58(9)	10	5.13(5)
20	2.76(4)	20	2.47(6)	20	1.04(1)	20	0.87(3)
40	0.66(2)	40	1.30(3)	40	0.36(1)	40	0.244(5)
60	0.288(8)	60	0.251(9)	60	0.112(5)	60	0.113(5)
80	0.121(4)	80	0.177(2)	80	0.098(2)	80	0.068(4)
100	0.103(2)	100	0.086(1)	100	0.085(3)	100	0.056(3)

Table S9. Variable temperature T_1 values of TRs in 0.01 (w/w) PMMA films.

PTM, film		**TTM, film**		**$TBr_3Cl_{10}M$, film**	
***T* / K**	**T_1/ ms**	***T* / K**	**T_1/ ms**	***T* / K**	**T_1/ ms**
10	13.4(2)	10	3.86(9)	10	0.86(3)
20	8.1(2)	20	0.97(2)	20	0.66(1)
40	2.85(5)	40	0.488(8)	40	0.366(5)
60	1.46(3)	60	0.426(4)	60	0.208(1)
80	0.753(6)	80	0.374(4)	80	0.176(1)
100	0.680(6)	100	0.278(3)	100	0.1110(6)
150	0.280(2)	150	0.200(2)	150	0.0829(6)
200	0.188(2)	200	0.167(1)	200	0.0171(2)
250	0.0302(5)	250	0.108(1)	250	0.0076(7)
298	0.0121(1)	298	0.01550(3)	298	0.00310(2)
TBr_3Cl_6M, film		**TBr_6Cl_5M, film**		**TTBrM, film**	
***T* / K**	**T_1/ ms**	***T* / K**	**T_1/ ms**	***T* / K**	**T_1/ ms**
10	0.229(8)	10	0.57(2)	10	1.060(8)
20	0.33(2)	20	0.64(2)	20	1.05(1)
40	0.233(5)	40	0.296(4)	40	0.280(3)
60	0.177(4)	60	0.157(3)	60	0.125(1)
80	0.147(4)	80	0.110(2)	80	0.112(1)
100	0.105(2)	100	0.081(1)	100	0.0609(4)
150	0.061(2)	150	0.0415(8)	150	0.049(1)
200	0.052(1)	200	0.0200(4)	200	0.0222(4)
250	0.0094(2)	250	0.0106(2)	250	0.0067(1)
298	0.00320(2)	298	0.00230(3)	298	0.00200(3)

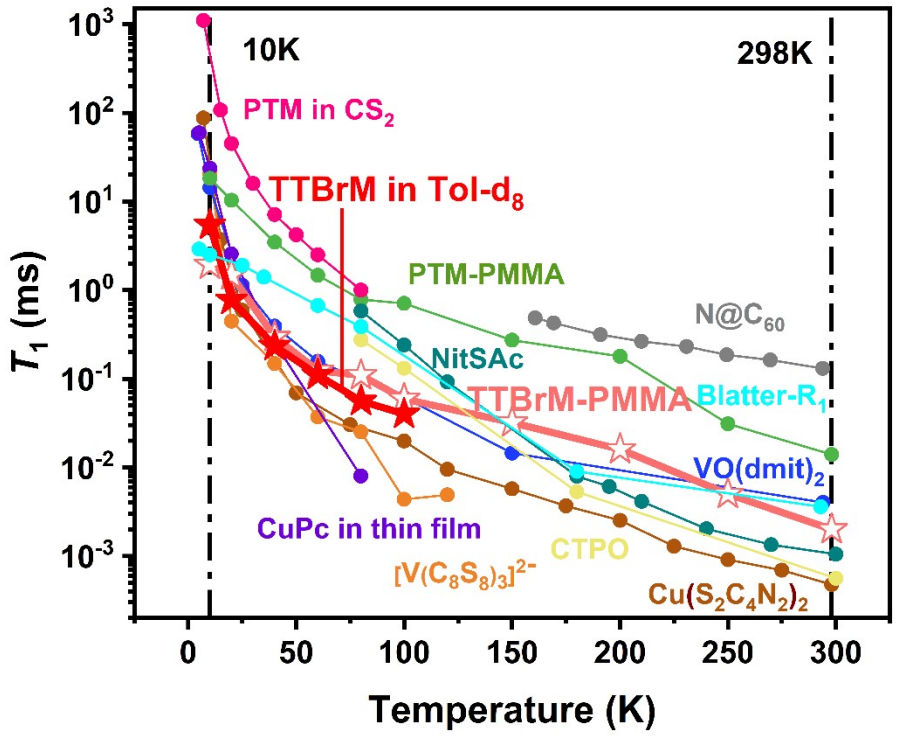

Figure S12. T_1 versus temperature measured by X-band pulsed-EPR (3460 G) for **TTBrM** in 0.1 mmol/L d_8-toluene solution and in 0.01 (w/w) PMMA film compared with other representative published molecule-based electronic spin qubit systems. Data are from ref. 2 ($N@C_{60}$, Gray)[2], ref. 3 (CuPc, Purple)[3], ref. 4 ($[V(C_8S_8)_3]^{2-}$, Orange)[4], ref. 5 ($VO(dmit)_2$, Dark Blue)[5], ref. 6 ($Cu(S_2C_4N_2)_2$, Brown)[6], ref. 7 (Blatter-R_1, Cyan)[7], ref. 8 (CTPO, Yellow; NitSAc, Dark Green)[8] and ref. 9 (PTM in CS_2, Pink)[9].

SI 4: T_m measurement and fitting for TRs

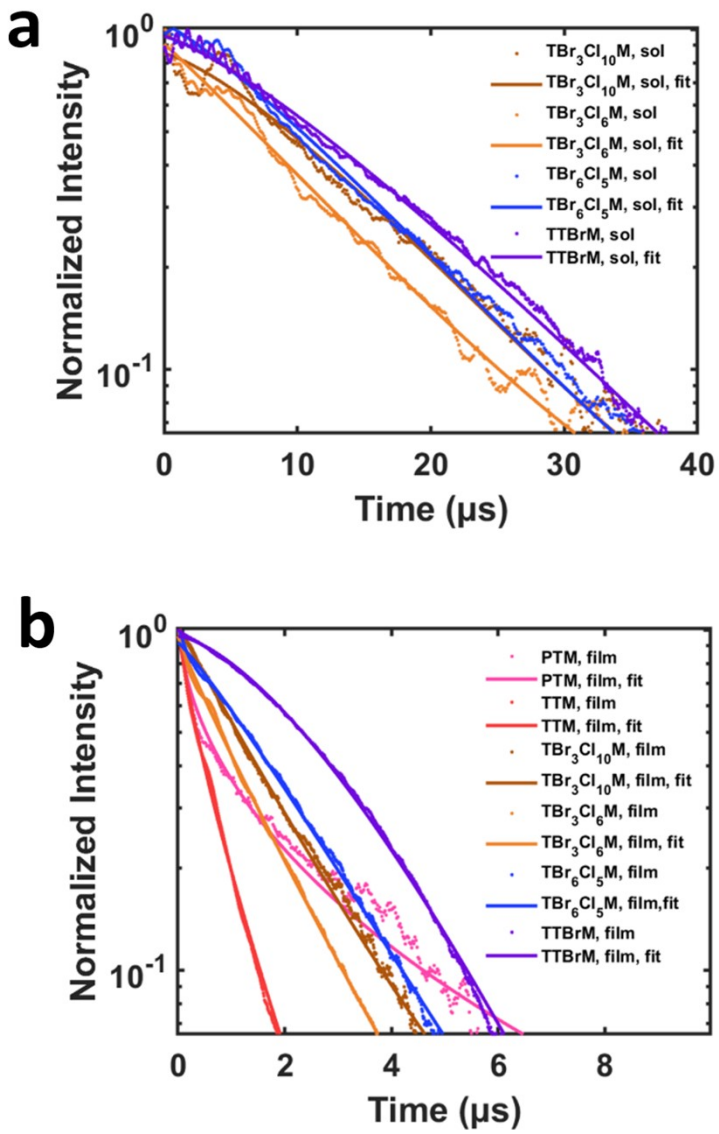

Figure S13. a) T_m of TRs in 0.1 mmol/L d_8-toluene frozen solutions in glassy state at 10 K and b) 0.01 (w/w) PMMA films at 10 K. (The data was smoothed with a five-point moving average).

All the Hahn-echo decay data are fitted with the stretched exponential decay function in Eq. S2. For the clarity of the graphs, we kept only the raw data and omitted the fitted curves in the following graphs.

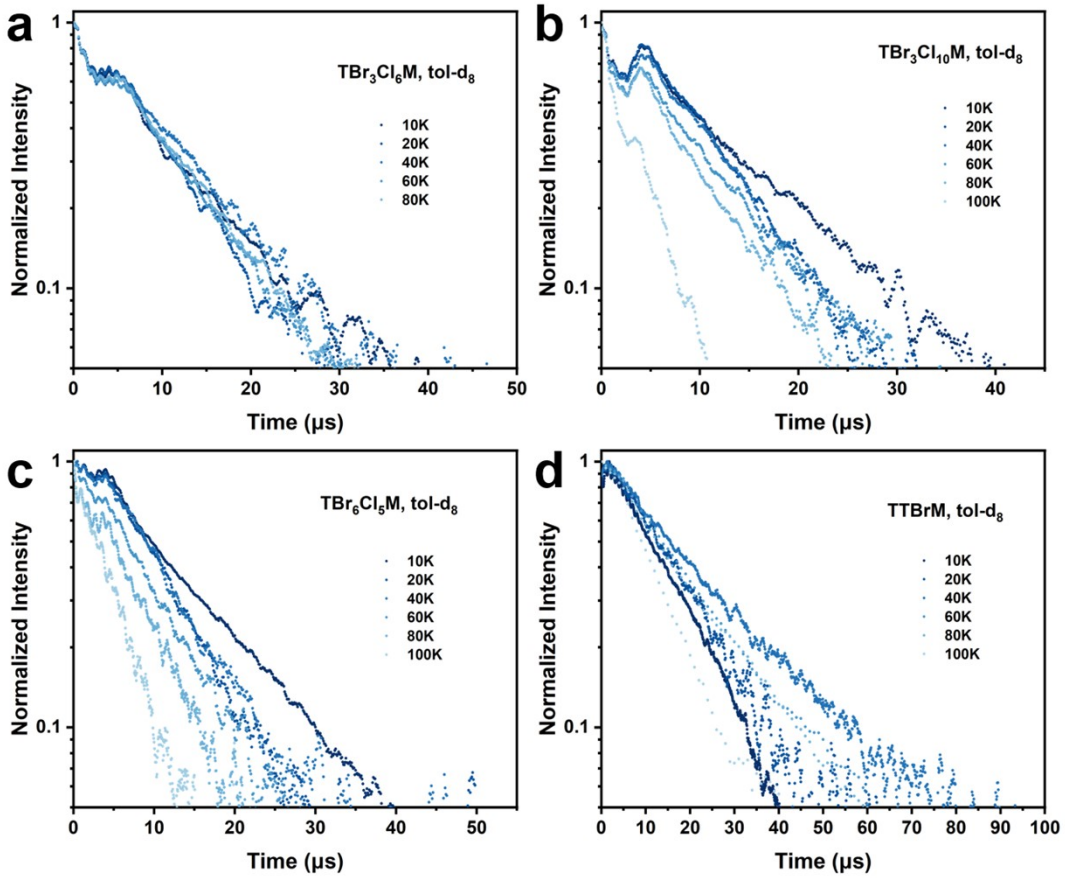

Figure S14. Variable temperature Hahn-echo decay data of TRs a) **TBr_3Cl_6M**, b) **$TBr_3Cl_{10}M$**, c) **TBr_6Cl_5M** and d) **TTBrM** in 0.1 mmol/L d_8-toluene frozen solutions in glassy state (The data was smoothed with a five-point moving average).

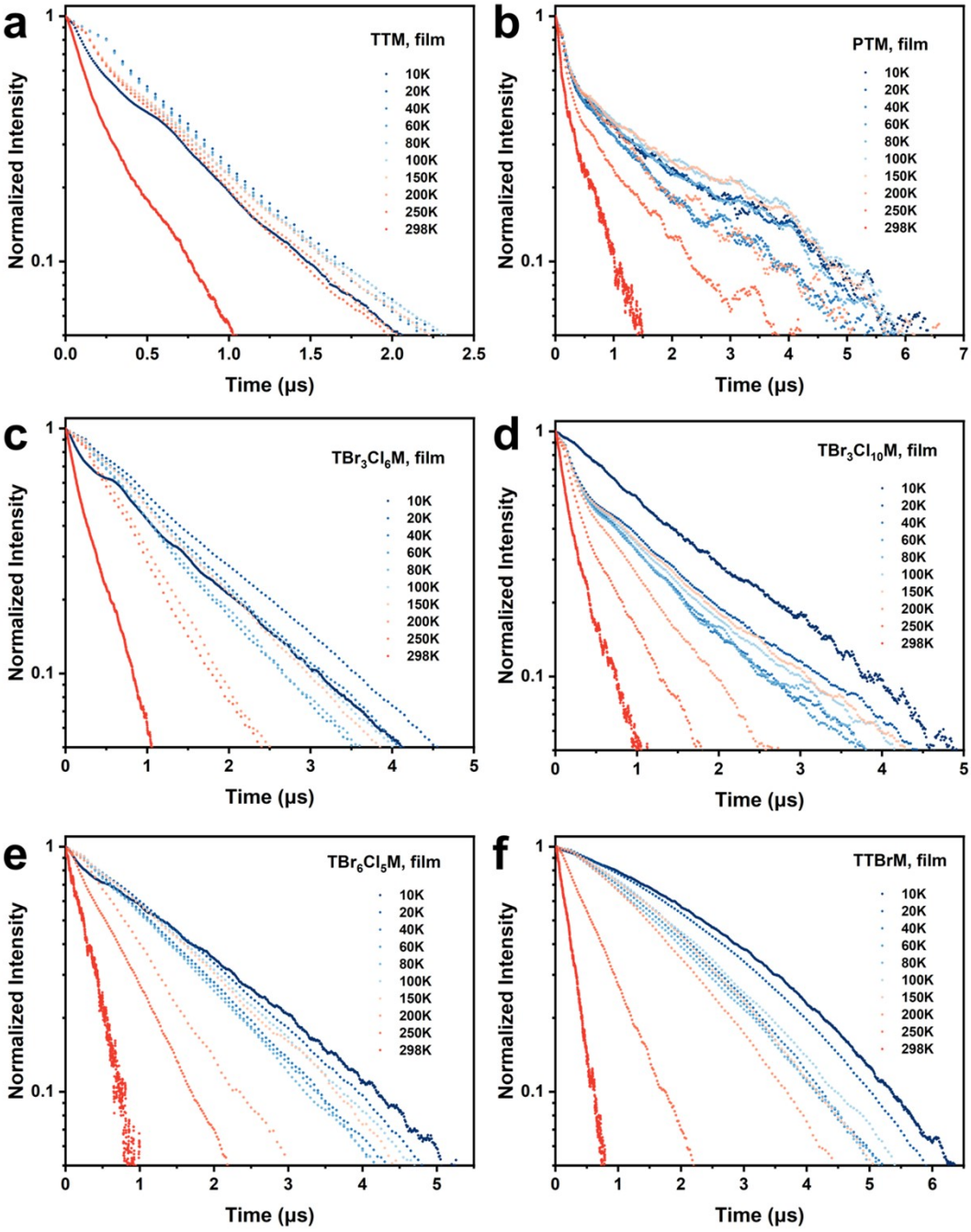

Figure S15. Variable temperature Hahn-echo decay data of TRs a) **TTM**, b) **PTM**, c) **TBr_3Cl_6M**, d) **$TBr_3Cl_{10}M$**, e) **TBr_6Cl_5M** and f) **TTBrM** in 0.01 (w/w) PMMA films (The data was smoothed with a five-point moving average).

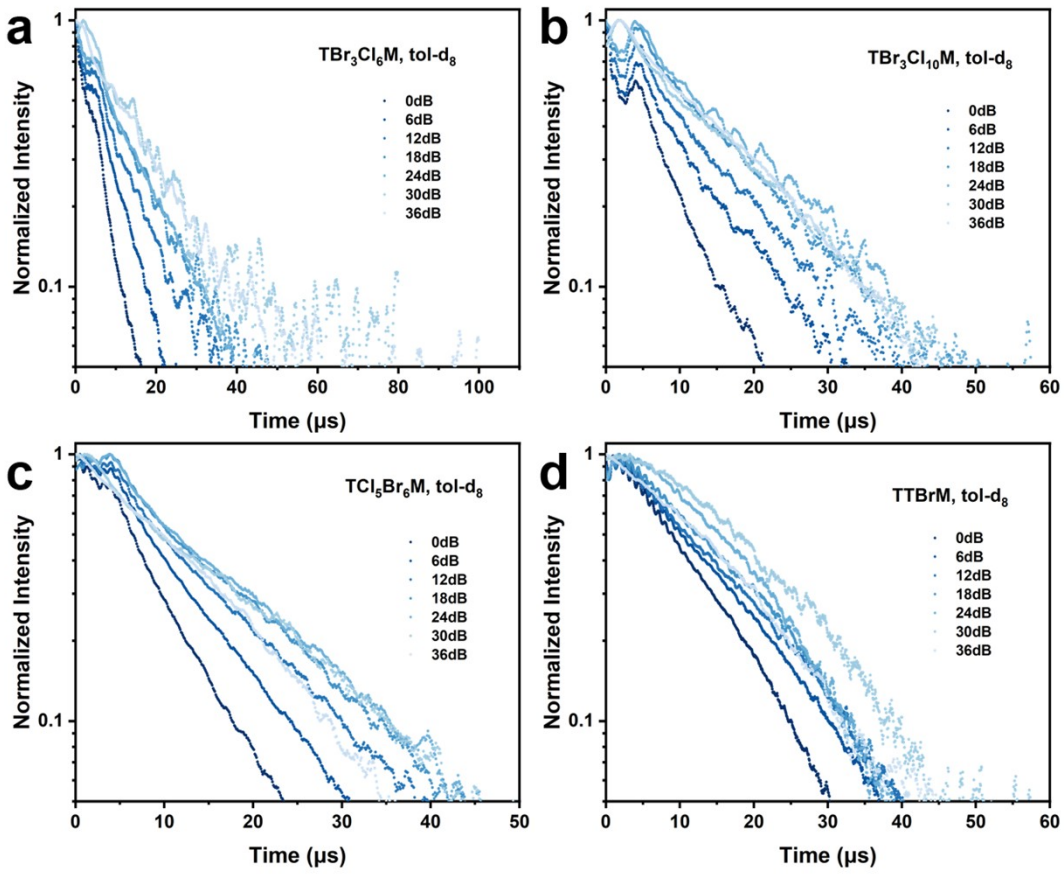

Figure S16. Variable microwave power Hahn-echo decay data of TRs a) **TBr_3Cl_6M**, b) **$TBr_3Cl_{10}M$**, c) **TCl_5Br_6M** and d) **TTBrM** in 0.1 mmol/L d_8-toluene frozen solutions in glassy state at 10 K (The data was smoothed with a five-point moving average).

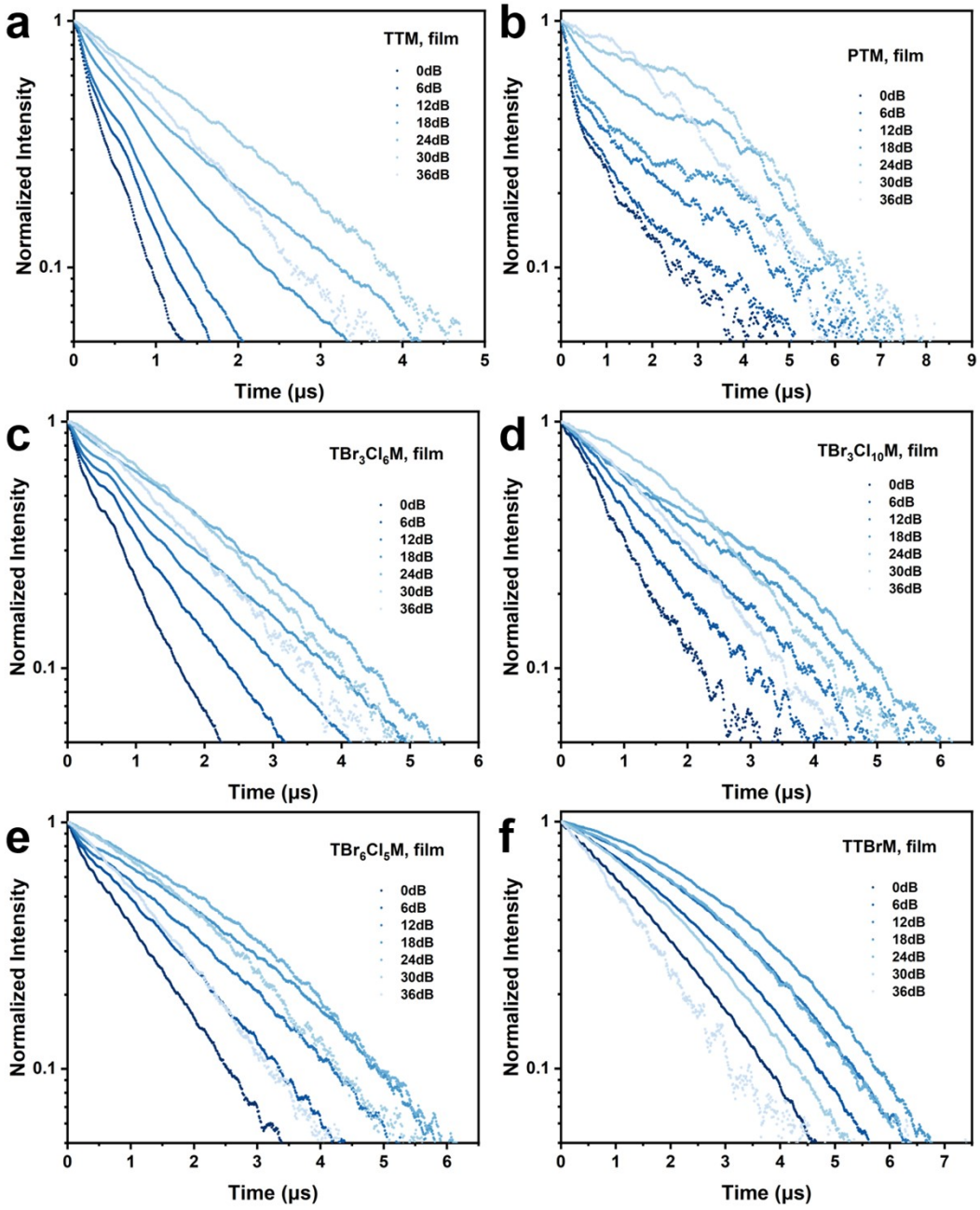

Figure S17. Variable microwave power Hahn-echo decay data of TRs a) **TTM**, b) **PTM**, c) **TBr_3Cl_6M**, d) **$TBr_3Cl_{10}M$**, e) **TBr_6Cl_5M** and f) **TTBrM** in 0.01 (w/w) PMMA films at 10 K (The data was smoothed with a five-point moving average).

Table S10. Variable temperature T_m values of TRs in 0.1 mmol/L d_8-toluene frozen solutions in glassy state.

$TBr_3Cl_{10}M$, sol.		**TBr_3Cl_6M, sol.**		**TBr_6Cl_5M, sol.**		**TTBrM, sol.**	
***T* / K**	**T_m/ µs**	***T* / K**	**T_m/ µs**	***T* / K**	**T_m/ µs**	***T* / K**	**T_m/ µs**
10	14.9(4)	10	10.9(2)	10	13.2(2)	10	16.3(1)
20	13.1(3)	20	11.2(2)	20	11.4(1)	20	17.6(2)
40	13.3(3)	40	12.8(3)	40	11.5(1)	40	21.1(2)
60	11.6(3)	60	11.1(2)	60	9.6(1)	60	18.3(5)
80	9.7(3)	80	11.5(2)	80	8.5(1)	80	17.0(5)
100	2.6(2)			100	5.0(1)	100	12.1(4)

Table S11. Variable temperature T_m values of TRs in 0.01 (w/w) PMMA films.

PTM, film		**TTM, film**		**$TBr_3Cl_{10}M$, film**	
***T* / K**	**T_m/ µs**	***T* / K**	**T_m/ µs**	***T* / K**	**T_m/ µs**
10	0.71(6)	10	0.511(6)	10	1.536(8)
20	0.4(1)	20	0.70 (1)	20	0.86(3)
40	0.41(4)	40	0.67(2)	40	0.70(2)
60	0.47(5)	60	0.68(1)	60	0.69(2)
80	0.5(1)	80	0.63(1)	80	0.67(2)
100	0.3(5)	100	0.580(8)	100	0.75(2)
150	0.7(3)	150	0.602(7)	150	0.81(2)
200	0.64(5)	200	0.577(7)	200	0.58(1)
250	0.25(3)	250	0.552(7)	250	0.35(1)
298	0.210(7)	298	0.206(2)	298	0.202(2)
TBr_3Cl_6M, film		**TBr_6Cl_5M, film**		**TTBrM, film**	
***T* / K**	**T_m/ µs**	***T* / K**	**T_m/ µs**	***T* / K**	**T_m/ µs**
10	1.261(7)	10	2.000(9)	10	3.102(5)
20	1.53(1)	20	1.844(9)	20	2.84(1)
40	1.34(1)	40	1.573(9)	40	2.304(5)
60	1.11(1)	60	1.529(9)	60	2.194(6)
80	1.14(1)	80	1.491(8)	80	2.074(7)
100	1.29(1)	100	1.735(8)	100	2.351(7)
150	1.29(1)	150	1.68(1)	150	2.259(6)
200	0.889(8)	200	1.03(1)	200	1.907(5)
250	0.81(1)	250	0.750(5)	250	0.753(6)
298	0.29(2)	298	0.397(9)	298	0.270(1)

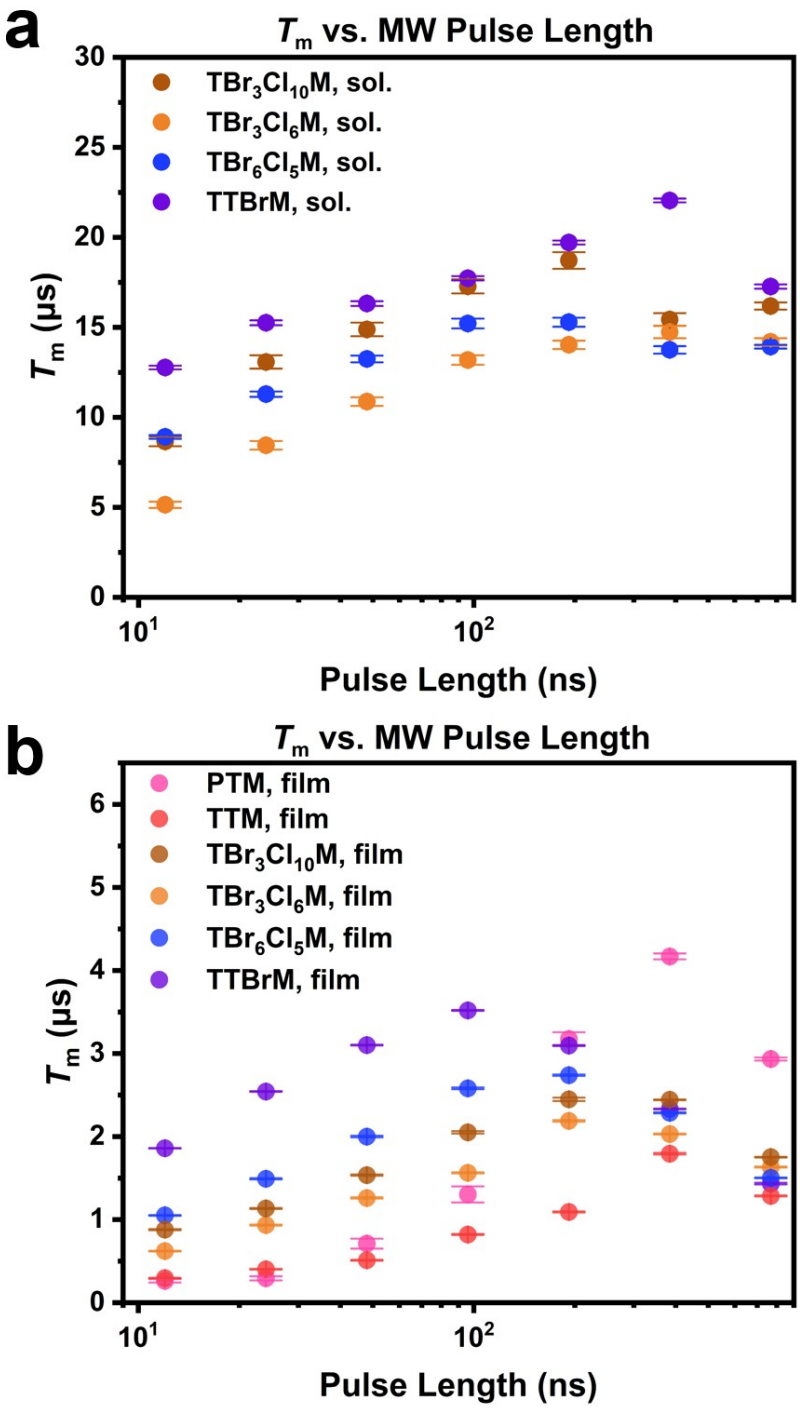

Figure S18. Variable-power T_m data of TRs a) in 0.1 mmol/L d_8-toluene frozen solutions in glassy state and b) in 0.01 (w/w) PMMA films at 10 K with π/2 pulse lengths adjusted to 12, 24, 48, 96, 192, 384, and 768 ns by 0, 6, 12, 18, 24, 30, and 36 dB attenuation. The error bars denote the standard error for each point, within the size range of the symbols.

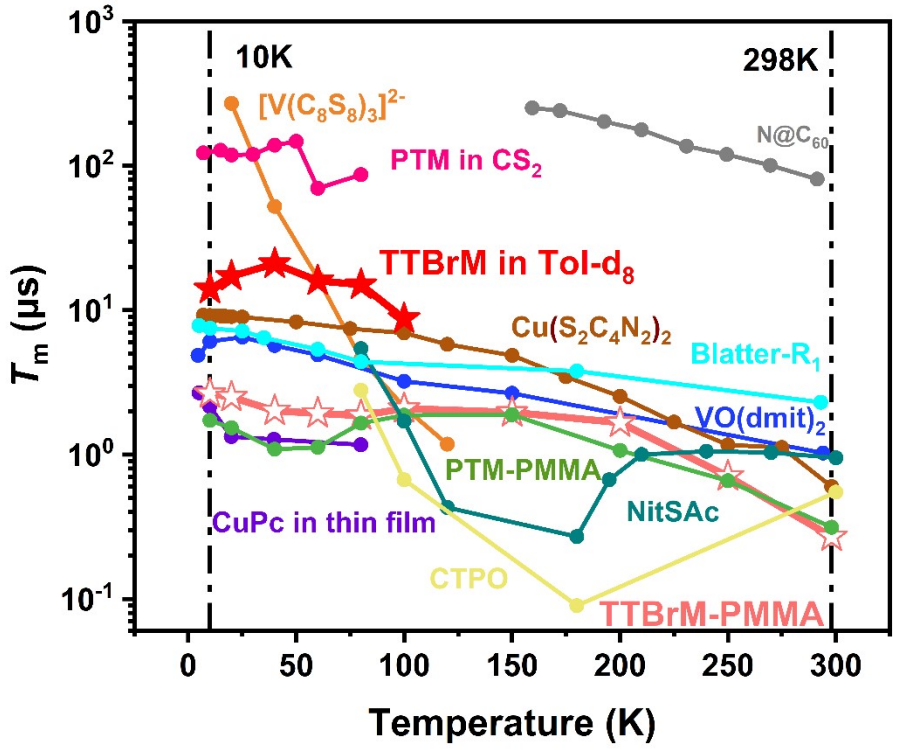

Figure S19. T_m versus temperature measured by X-band pulsed-EPR (3460 G) for **TTBrM** in 0.1 mmol/L d_8-toluene solution and in 0.01 (w/w) PMMA film compared with other representative published molecule-based electronic spin qubit systems. Data are from ref. 2 ($N@C_{60}$, Gray)[2], ref. 3 (CuPc, Purple)[3], ref. 4 ($[V(C_8S_8)_3]^{2-}$, Orange)[4], ref. 5 ($VO(dmit)_2$, Blue)[5] and ref. 6 ($Cu(S_2C_4N_2)_2$, Brown)[6], ref. 7 (Blatter-R_1, Cyan)[7], ref. 8 (CTPO, Yellow; NitSAc, Dark Green)[8] and ref. 9 (PTM in CS_2, Pink)[9].

SI 5: Rabi oscillations of TRs

Introduction to the nature of rabi oscillations

For such organic radicals of spin-1/2 with two energy levels, the Hamiltonian $\hat{H}_0$ under the external static magnetic field B_0 along z-axis can be expressed as,

$\hat{H}_0 = \mu_B g_z B_0 \hat{S}_z = \omega_0 \hat{S}_z, \#(Eq.\ S3)$

where μ_B is the Bohr magneton, g_z is the g-matrix's principal value along the z-axis, $\hat{S}_z$ is the spin operator along the z-axis and $\omega_0 = \mu_B g_z B_0$ is the Larmor frequency of the electron spin in the static magnetic field B_0. The two eigenstates of the system under $\hat{H}_0$ are $|\psi_{\pm}^{z}\rangle = \left|\pm\frac{1}{2}, z\right\rangle$. Although the two-level system is in thermal equilibrium by Boltzmann population, considering the pseudo-pure state, the system is initially prepared to the lower energy eigenstate $|\psi_0\rangle = |\psi_{+}^{z}\rangle$, and the spin-1/2 system can be demonstrated in the Bloch sphere (Figure S20).

In the existence of microwave magnetic field B_1 along the x-direction, the Hamiltonian of $\hat{H}_1$ is time-dependent,

$\hat{H}_1(t) = \mu_B g_x B_1 \hat{S}_x \cos(2\pi\Omega t) = \omega_1 \hat{S}_x \cos(2\pi\Omega t), \#(Eq.\ S4)$

where g_x is the g-matrix's principal value along the x-axis, Ω is the microwave frequency, $\omega_1 = \mu_B g_x B_1$ is the Larmor frequency of the electron spin in a magnetic field B_1 along the x-axis, and $\hat{S}_x$ is the spin operator along the x-axis. The total Hamiltonian $\hat{H}_{Tot}(t)$ of the system therefore turns out to be time-dependent as well,

$\hat{H}_{Tot}(t) = \hat{H}_0 + \hat{H}_1(t). \#(Eq.\ S5)$

In the purpose of convenient treatment of the Hamiltonian as time-independent, the rotating frame and rotation-wave approximation are considered. Applying the resonance condition, $\Omega = \omega_0$, the total Hamiltonian $\hat{H}_{Tot}^{'}$ turns out to be

$\hat{H}_{Tot}^{'} = \omega_1 \hat{S}_x = \mu_B g_x B_1 \hat{S}_x. \#(Eq.\ S6)$

Note that the eigenstate of the system under the $\hat{H}_{Tot}^{'}$ is no longer $|\psi_{\pm}^{z}\rangle$, but superpositions of them, $|\psi_{\pm}^{x}\rangle = \left|\pm\frac{1}{2}, x\right\rangle = \frac{1}{\sqrt{2}}\left(|\psi_{+}^{z}\rangle \pm |\psi_{-}^{z}\rangle\right)$. Therefore, the initial state

$|\psi_0\rangle = |\psi^z_+\rangle$, which is the eigenstate of $\hat{H}_0$, is now a superposition of $|\psi^x_\pm\rangle$ under $\hat{H}_{Tot}$, denoted as $|\psi_0\rangle = |\psi^z_+\rangle = \frac{1}{\sqrt{2}}(|\psi^x_+\rangle + |\psi^x_-\rangle)$. This superposition state evolves to $|\psi_t\rangle$ following the time-dependent Schrödinger equation,

$$|\psi_t\rangle = e^{-i\hat{H}_1 t}|\psi_0\rangle = \frac{1}{\sqrt{2}}\left[e^{-iE_+ t}|\psi^x_+\rangle + e^{-iE_- t}|\psi^x_-\rangle\right], \#(Eq.\,S7)$$

where $E_\pm$ are the energies of $|\psi^x_\pm\rangle$. Therefore, the Rabi oscillation, realized by applying the nutation microwave pulse $\hat{H}_1(t)$, is fundamentally the coherent quantum phase evolution as described by **Eq. S6**. The possibilities of the superposition state $|\psi_t\rangle$ collapses to the eigenstates of $\hat{H}_0$, $|\psi^z_\pm\rangle$ then oscillates upon time. In this sense, one can regard the nutation experiment as an illustration of the ability to prepare arbitrary coherent quantum superposition state with these organic radicals as spin-1/2 systems, which is a prerequisite for the realization of QIP. The Rabi frequency can be calculated as the frequency in the oscillation of the possibility $|\langle\psi^z_+|\psi_t\rangle|^2$, which is given by

$$\omega_{Rabi} = \omega_1 = E_+ - E_- = \mu_B g_x B_1 \sqrt{S(S+1) - M_S(M_S+1)}. \#(Eq.\,S8)$$

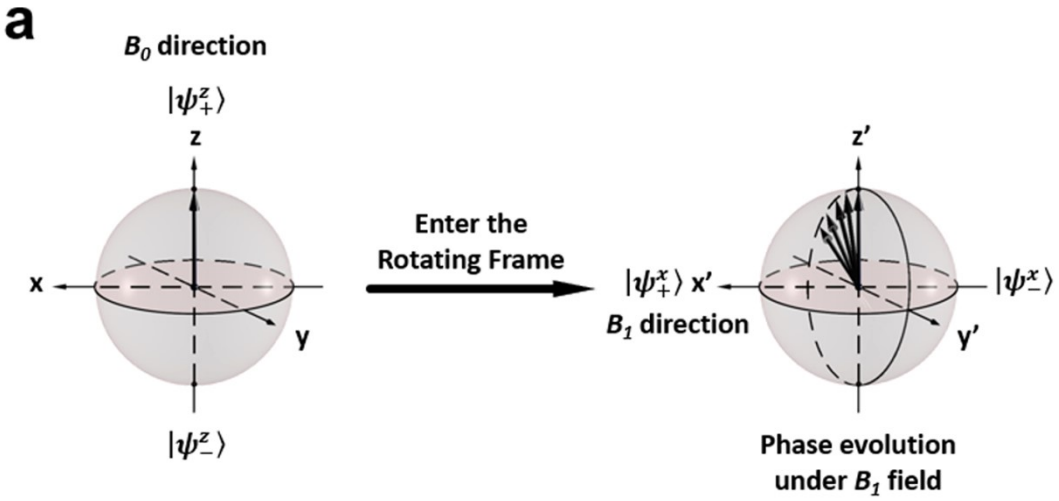

Scheme S4. a) Transform the experimental frame into rotating frame with rotating wave approximation. The eigenstates transform from $|\psi^z_\pm\rangle$ to $|\psi^x_\pm\rangle$ by eliminating the influence of B_0 field while retaining B_1 field in Bloch sphere.

Rabi oscillation data of TRs

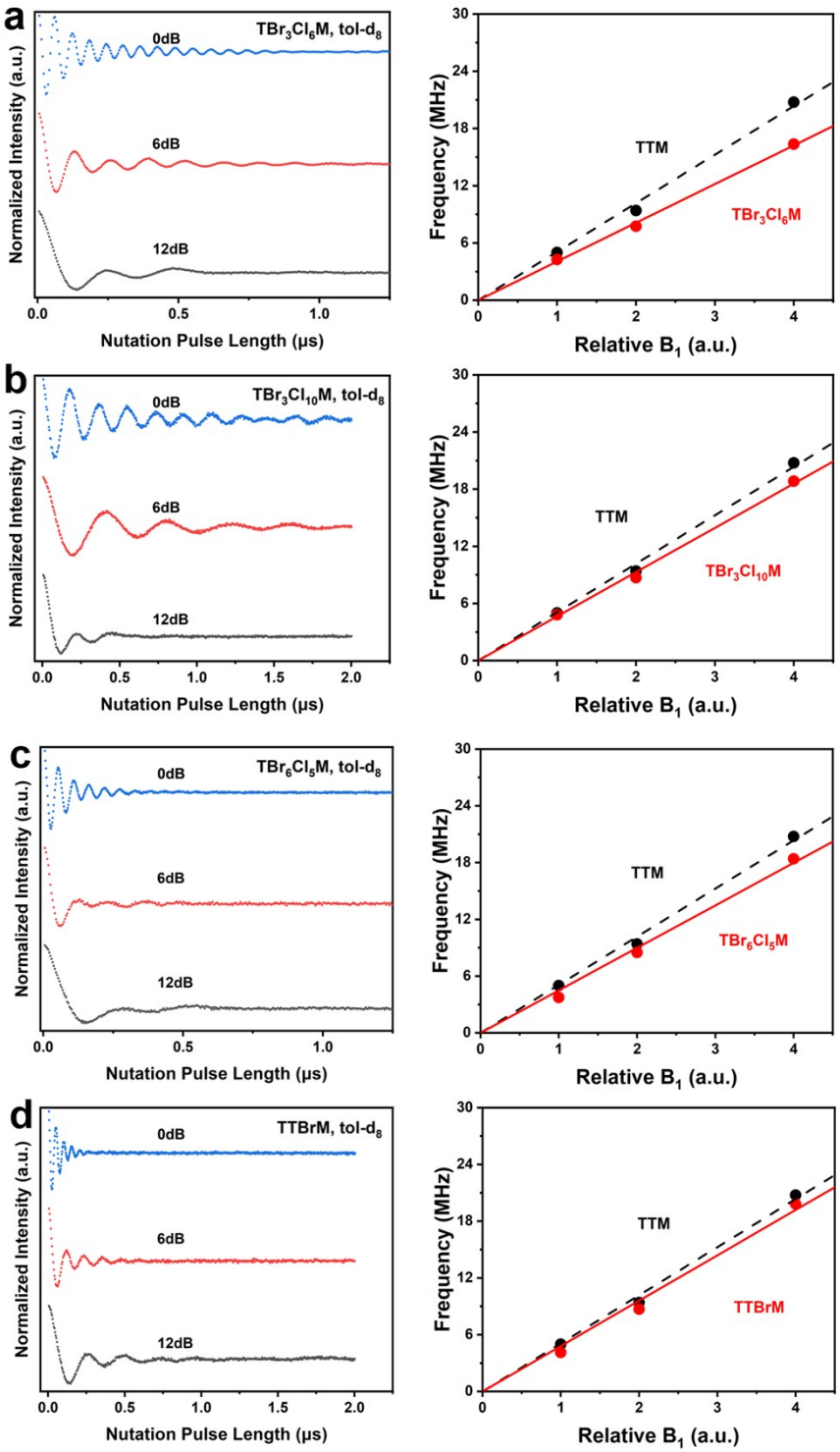

Figure S20. Variable B_1 Rabi oscillation data of TRs a) **TBr_3Cl_6M**, b) **$TBr_3Cl_{10}M$**, c)

TCl_5Br_6M and d) **TTBrM** in 0.1 mmol/L d_8-toluene frozen solutions in glassy state at 10 K. The Rabi frequencies (Ω_R) show a linear function of the magnetic field of microwave (B_1).

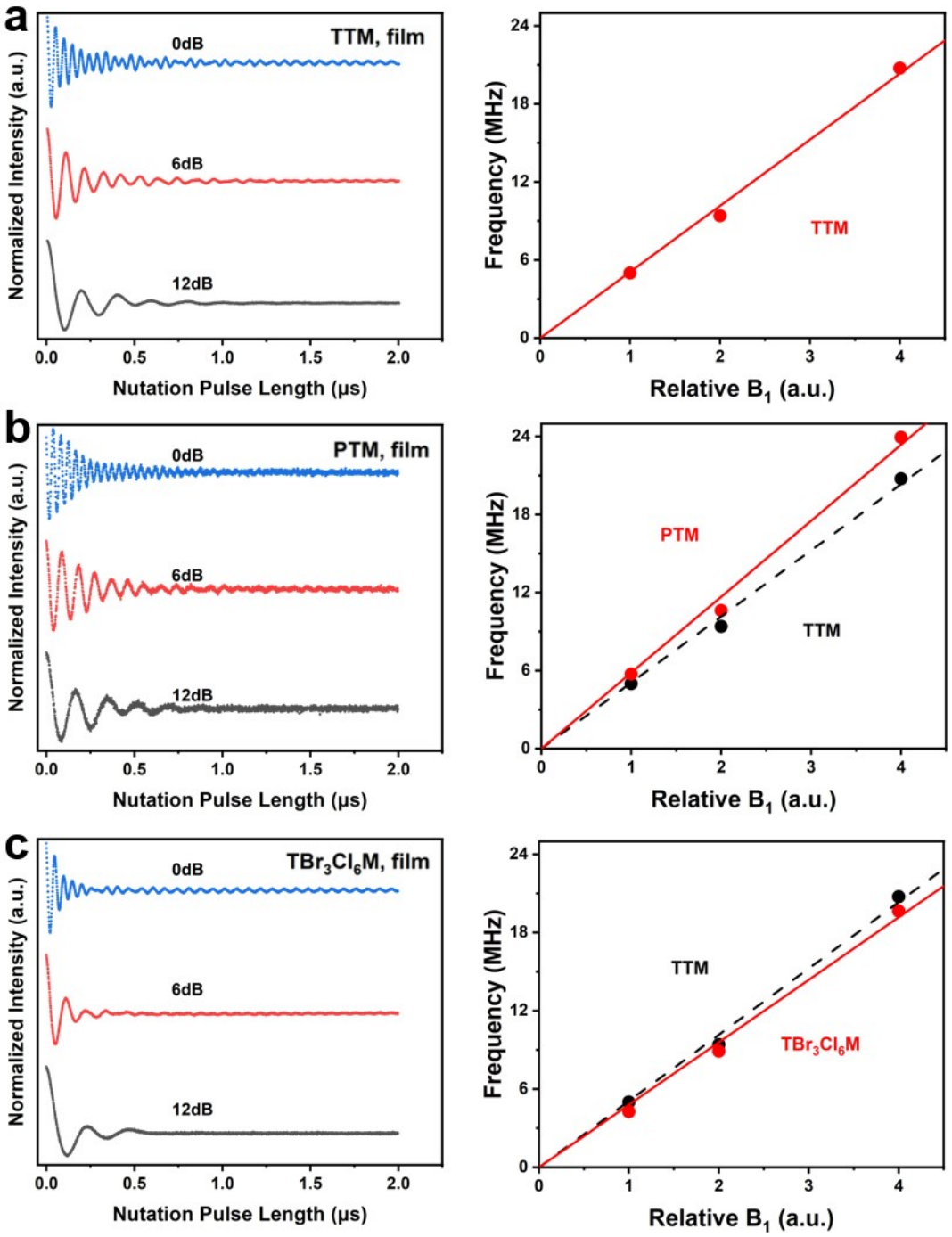

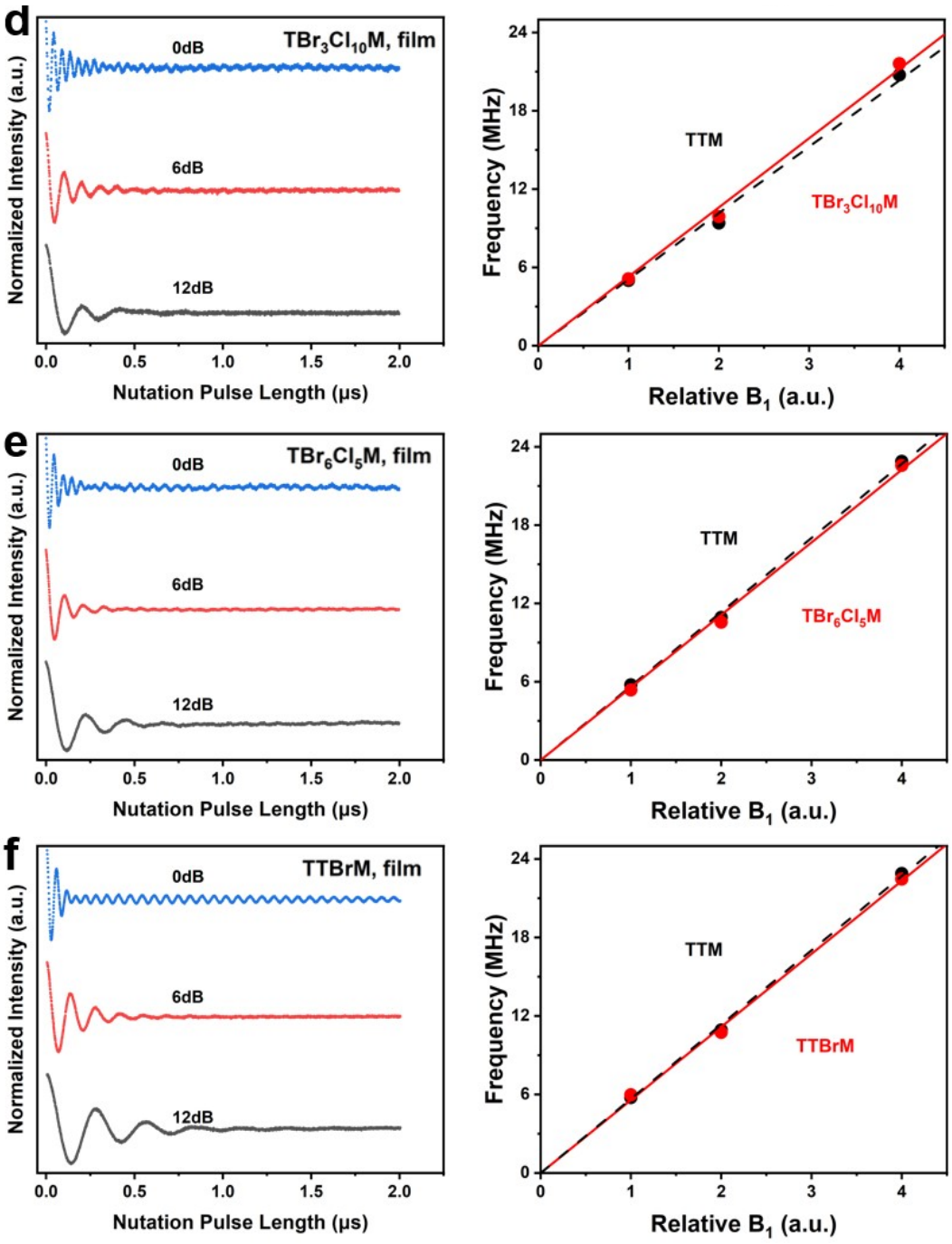

Figure S21. Variable B_1 Rabi oscillation data of TRs a) **TTM**, b) **PTM**, c) **TBr_3Cl_6M**, d) **$TBr_3Cl_{10}M$**, e) **TCl_5Br_6M** and f) **TTBrM** in 0.01 (w/w) PMMA films at 10 K. The Rabi frequencies (Ω_R) show a linear function of the magnetic field of microwave (B_1).

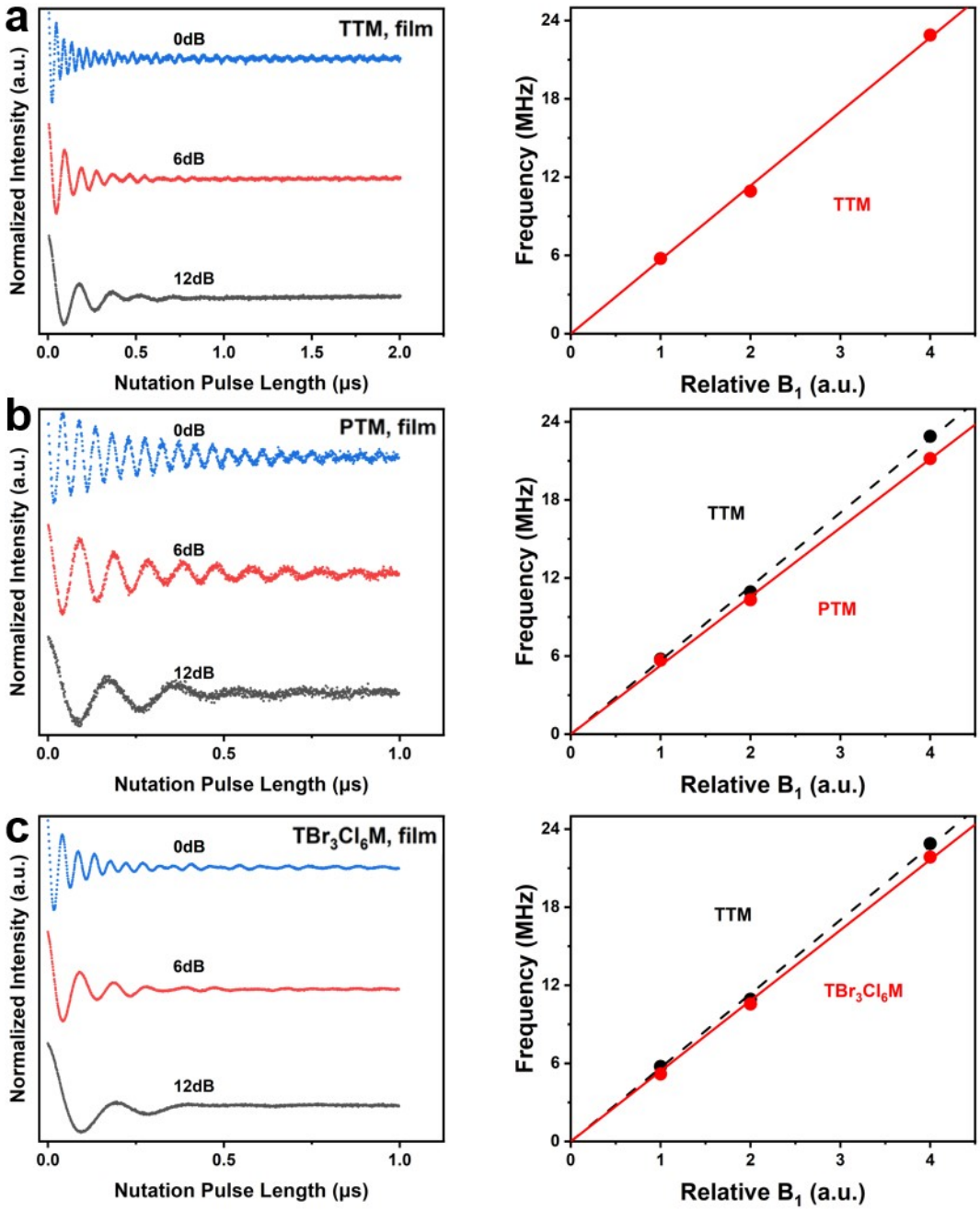
a
TTM, film
0dB
6dB
12dB
Normalized Intensity (a.u.)
Nutation Pulse Length (μs)
0.0
0.5
1.0
1.5
2.0
Frequency (MHz)
Relative B1 (a.u.)
TTM
0
6
12
18
24
0
1
2
3
4
b
PTM, film
0dB
6dB
12dB
Normalized Intensity (a.u.)
Nutation Pulse Length (μs)
0.0
0.5
1.0
TTM
PTM
Frequency (MHz)
Relative B1 (a.u.)
c
TBr3Cl6M, film
0dB
6dB
12dB
Normalized Intensity (a.u.)
Nutation Pulse Length (μs)
0.0
0.5
1.0
TTM
TBr3Cl6M
Frequency (MHz)
Relative B1 (a.u.)

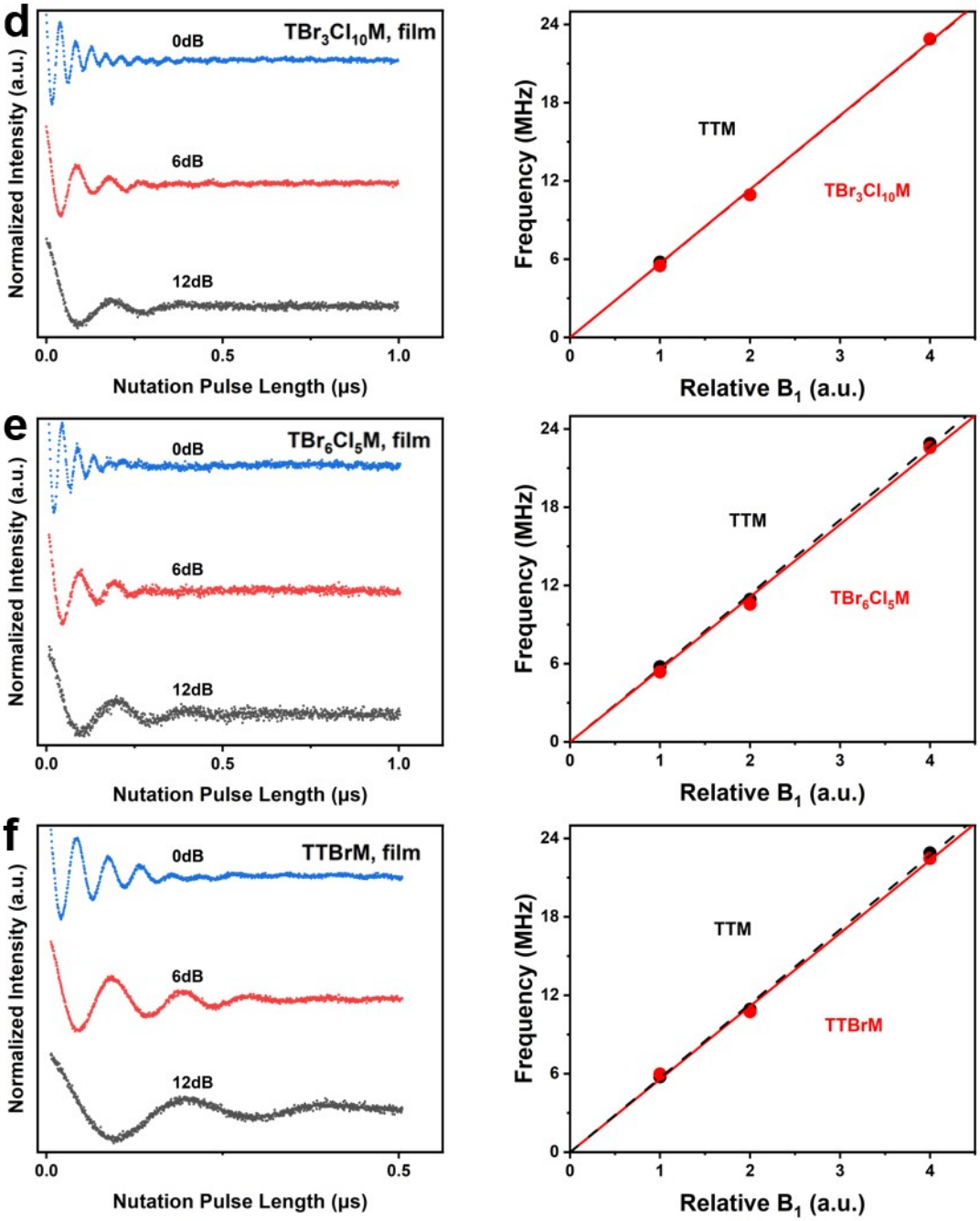

Figure S22. Variable B_1 Rabi oscillation data of TRs a) **TTM**, b) **PTM**, c) **TBr_3Cl_6M**, d) **$TBr_3Cl_{10}M$**, e) **TBr_6Cl_5M** and f) **TTBrM** in 0.01 (w/w) PMMA films at room temperature. The Rabi frequencies (Ω_R) show a linear function of the magnetic field of microwave (B_1).

SI 6: Simulations of T_m measurement with CPMG dynamic decoupling for TRs

All the CPMG data can be fitted with the stretched exponential decay function in Eq. S2. For the sake of simplicity and aesthetics of the graphs, we kept only the raw data and omitted the fitted curves in the following graphs.

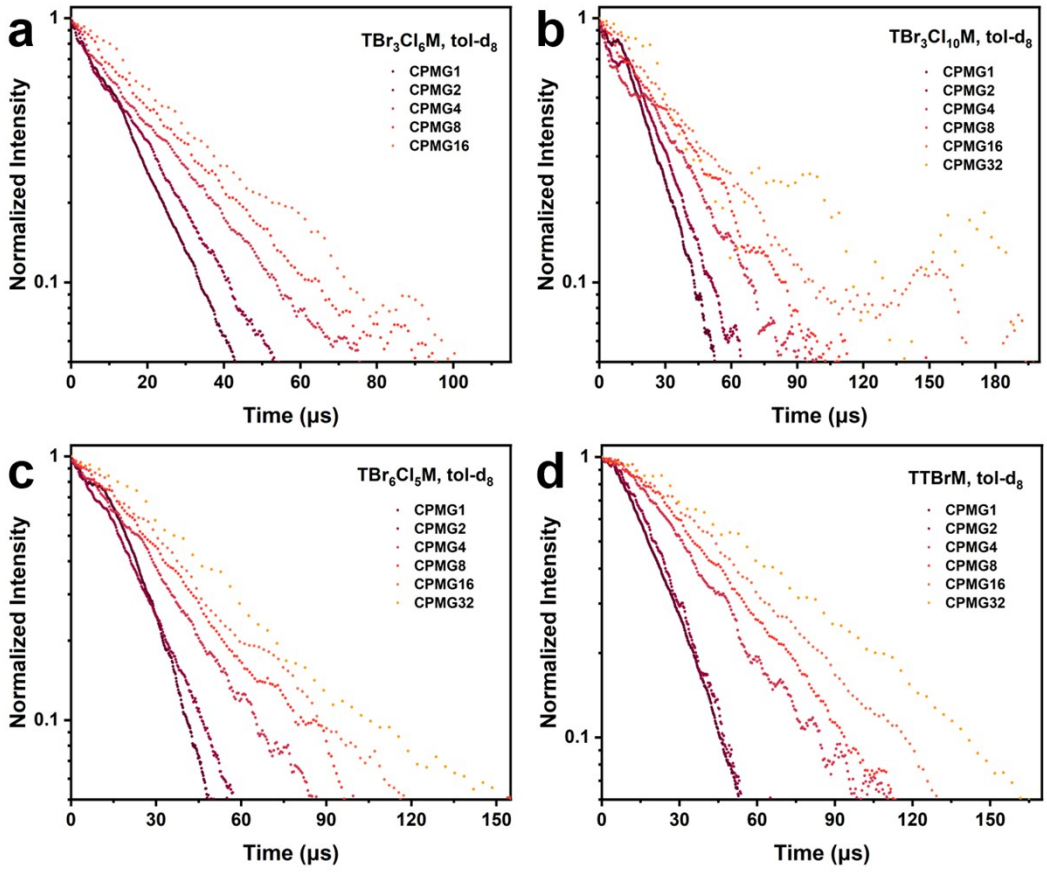

Figure S23. CPMG data of TRs a) **TBr_3Cl_6M**, b) **$TBr_3Cl_{10}M$**, c) **TBr_6Cl_5M** and d) **TTBrM** in 0.1 mmol/L d_8-toluene frozen solutions in glassy state at 10 K (The data was smoothed with a five-point moving average).

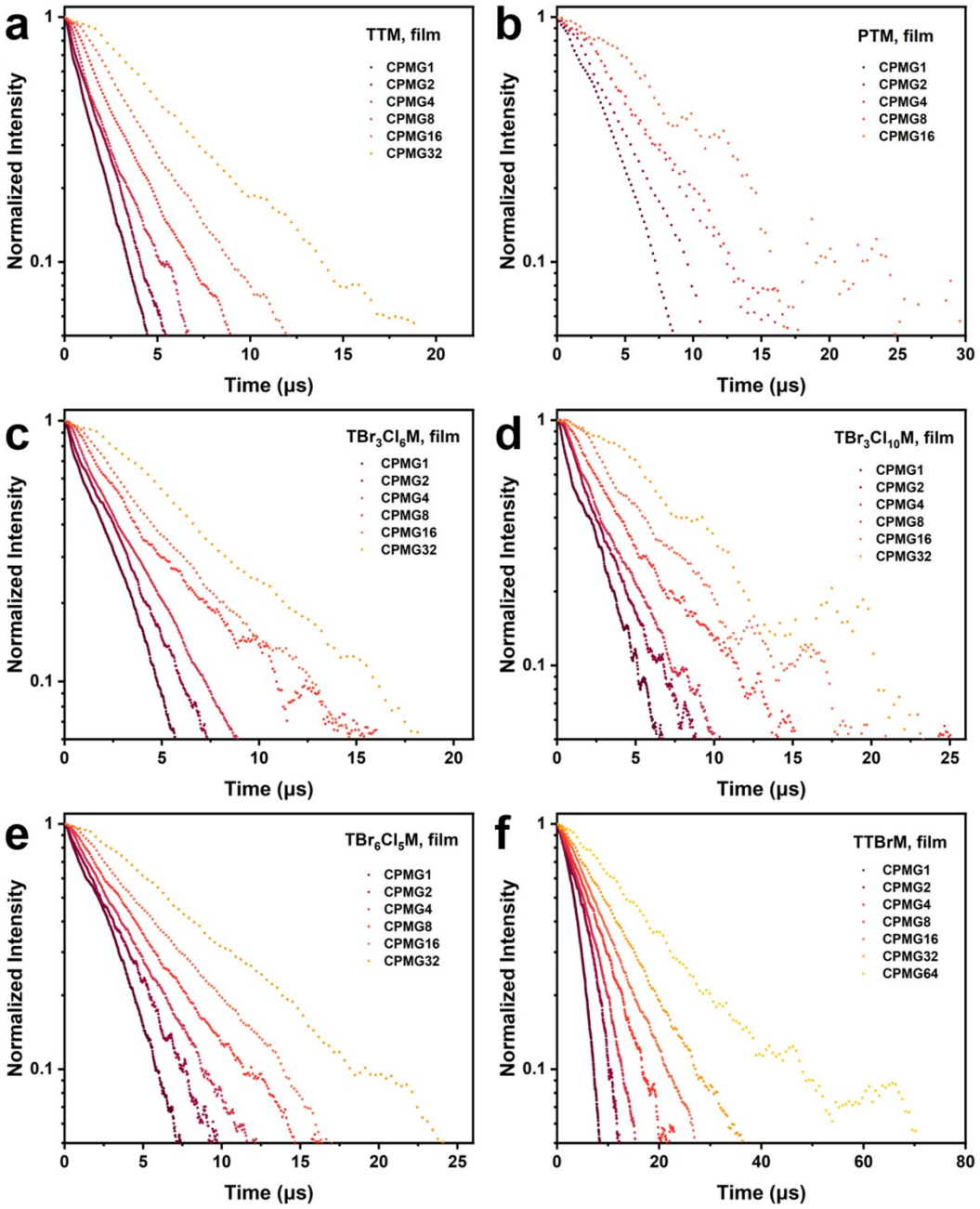

Figure S24. CPMG data of TRs a) **TTM**, b) **PTM**, c) **TBr_3Cl_6M**, d) **$TBr_3Cl_{10}M$**, e) **TBr_6Cl_5M** and f) **TTBrM** in 0.01 (w/w) PMMA films at 10 K (The data was smoothed with a five-point moving average).

Table S12. T_m values from CPMG experiments of TRs in 0.1 mmol/L d_8-toluene frozen solutions in glassy state.

$TBr_3Cl_{10}M$, sol.		TBr_3Cl_6M, sol.		TBr_6Cl_5M, sol.		TTBrM, sol.	
Inversion pulse number	**T_m/ µs**	**Inversion pulse number**	**T_m/ µs**	**Inversion pulse number**	**T_m/ µs**	**Inversion pulse number**	**T_m/ µs**
1	24.8(2)	1	16.8(1)	1	25.7(2)	1	23.9(1)
2	30.3(4)	2	17.9(3)	2	24.1(2)	2	26.3(2)
4	34.8(9)	4	21.6(3)	4	30.9(3)	4	38.6(3)
8	37.2(8)	8	25.1(5)	8	35.8(4)	8	47.2(4)
16	37(2)	16	30.2(9)	16	39.4(9)	16	55.7(7)
32	34(6)	32	33(2)	32	48(1)	32	70(1)

Table S13. T_m values from CPMG experiments of TRs in 0.01 (w/w) PMMA films.

PTM, film		TTM, film		$TBr_3Cl_{10}M$, film	
Inversion pulse number	**T_m/ µs**	**Inversion pulse number**	**T_m/ µs**	**Inversion pulse number**	**T_m/ µs**
1	3.86(4)	1	1.333(9)	1	1.99(3)
2	4.6(1)	2	1.74(1)	2	2.50(2)
4	6.1(1)	4	1.81(3)	4	2.80(3)
8	6.2(2)	8	2.69(4)	8	3.92(8)
16	9.0(4)	16	3.81(8)	16	5.3(2)
		32	5.9(1)	32	8.2(4)
TBr3Cl6M, film		**TBr6Cl5M, film**		**TTBrM, film**	
Inversion pulse number	**T_m/ µs**	**Inversion pulse number**	**T_m/ µs**	**Inversion pulse number**	**T_m/ µs**
1	2.16(2)	1	2.95(2)	1	4.29(1)
2	2.62(2)	2	3.31(2)	2	6.08(3)
4	2.85(2)	4	3.75(2)	4	6.82(2)
8	3.62(6)	8	4.55(4)	8	8.09(3)
16	4.67(9)	16	6.01(9)	16	9.48(5)
32	7.0(1)	32	8.7(2)	32	12.0(1)
64	10(1)			64	17.8(5)

Reference

[1] M. Ballester, J. Riera, J. Castañer, C. Rovira and O. Armet, *Synthesis*, 1986, **1986**, 64–66.

[2] J. J. L. Morton, A. M. Tyryshkin, A. Ardavan, K. Porfyrakis, S. A. Lyon and G. Andrew D. Briggs, *J. Chem. Phys.*, 2006, **124**, 014508.

[3] M. Warner, S. Din, I. S. Tupitsyn, G. W. Morley, A. M. Stoneham, J. A. Gardener, Z. Wu, A. J. Fisher, S. Heutz, C. W. M. Kay and G. Aeppli, *Nature*, 2013, **503**, 504–508.

[4] J. M. Zadrozny, J. Niklas, O. G. Poluektov and D. E. Freedman, *ACS Cent. Sci.*, 2015, **1**, 488–492.

[5] M. Atzori, E. Morra, L. Tesi, A. Albino, M. Chiesa, L. Sorace and R. Sessoli, *J. Am. Chem. Soc.*, 2016, **138**, 11234–11244.

[6] K. Bader, D. Dengler, S. Lenz, B. Endeward, S.-D. Jiang, P. Neugebauer and J. Van Slageren, *Nat. Commun.*, 2014, **5**, 5304.

[7] A. S. Poryvaev, E. Gjuzi, D. M. Polyukhov, F. Hoffmann, M. Fröba and M. V. Fedin, *Angew. Chem. - Int. Ed.*, 2021, **60**, 8683–8688.

[8] A. Collauto, M. Mannini, L. Sorace, A. Barbon, M. Brustolon and D. Gatteschi, *J. Mater. Chem.*, 2012, **22**, 22272.

[9] D. Schäfter, J. Wischnat, L. Tesi, J. A. De Sousa, E. Little, J. McGuire, M. Mas-Torrent, C. Rovira, J. Veciana, F. Tuna, N. Crivillers and J. Van Slageren, *Adv. Mater.*, 2023, **35**, 2302114.